PRECISION MEASUREMENT OF NUCLEAR ENERGIES USING THE NON-FERROMAGNETIC BETA-RAY SPECTROMETER WITH HOMOGENEOUS MAGNETIC FIELD

Thesis by

James Reed Wilts

In Partial Fulfillment of the Requirements

for the Degree of

Doctor of Philosophy

California Institute of Technology

Pasadena, California

1952

ACKNOWLEDGEMENTS

The construction of the new beta-ray spectrometer was accomplished through the efforts of many individuals. The author is indebted to each of these persons. In particular, the author wishes to express his appreciation to Mr. James L. Kohl and to Mr. Louis Bogart, who have assisted in many important ways with the instrumentation of the new spectrometer.

The helpful advice and assistance of Dr. David E. Muller are also gratefully acknowledged.

Foremost, however, the author is indebted to Professor J. W. M. DuMond, whose inspiration made this work possible, and whose advice and encouragement have been invaluable.

Many drawings and photographs have been taken from earlier reports on the instrument. Appreciation is expressed to Mr. Larry Harmon, who kindly provided the author with a darkroom and an enlarger.

The author also wishes to thank his wife for her patient assistance in revising the manuscript and in typing the final draft.

Financial grants from the Research Corporation made possible the construction of the spectrometer. The work was also assisted by the joint program of the Office of Naval Research and the Atomic Energy Commission.

ABSTRACT

A new precision magnetic beta-ray spectrometer achieving simultaneously both high resolution and high luminosity is presented. The theory of its operation and design by Professor J. W. M. DuMond is traced.

Successful adaptation of a resonance absorption scheme using the magnetic moment of the proton for precisely measuring and controlling the magnetic field is reported.

The instrumental line profile is discussed. A new type of source due to Dr. D. E. Muller is shown to simplify the interpretation of experimental data by giving the spectral lines obtained from the conversion of nuclear gamma-rays a characteristic fiducial feature of high reproducibility.

The reproducibility of measurements claimed for the instrument is verified by the results of a study of the Thorium F and I lines. Repeated observations having a standard deviation for a single observation of less than one part in 10,000. are obtained.

TABLE OF CONTENTS

Part	Title	Page
I	THE THEORY OF THE DESIGN OF THE SPECTROMETER	
	A. Introduction	1
	B. The Determination of the Ultimate Intersection of Two Coalescing Traces	5
	C. The Determination of the Co-latitude Angle Optimizing the Luminosity for a Specified Resolution	6
	D. The Dimensions of the Ultimate Trace of the Spectrometer	9
II	THE CONSTRUCTION OF THE SPECTROMETER	
	A. The General Features of the Spectrometer . .	11
	B. The Source Assembly	14
	C. The Radiation Detector	17
III	THE MEASUREMENT AND CONTROL OF THE MAGNETIC FIELD	
	A. The Operation of the Proton-Moment Circuit .	21
	1. The Resonance Heads	28
	a. The Sweep Coils	30
	b. The Radio Frequency Coil	31
	2. The Radio-Frequency Oscillator Unit . . .	36
	3. The Audio Oscillator and Phase Sensitive Detector	43
	B. The Magnetic Field Regulator	46

ILLUSTRATIONS

Figure No.	Title	Page
1	The Trajectory in Three Views and Its Trace	2
2	The Ultimate Intersection of Two Coalescing Traces	4
3	The Dimensions of the Ultimate Trace In Inches	10
4	Complete Cross-Section View of the Homogeneous Magnetic Field Beta-Ray Spectrometer	12
5	The Source-Centering Jig	16
6	The Perforated Tube Geiger-Muller Counter	18
7	The Homogeneous Magnetic Field Beta-Ray Spectrometer	20
8	Block Diagram of Proton Resonance Units	26
9	Scale Drawing of the Largest Resonance Head	29
10	The Axial Variation of the Field of Double-Helmholz Sweep Coils	32
11	Top View of the Proton Resonance Oscillator	37
12	Bottom View of the Proton Resonance Oscillator	38
13	Schematic of the Proton Resonance R-F Oscillator Unit	39
14	Schematic of Phase and Amplitude Controls for the Audio Oscillator . . .	45
15	Schematic of the Phase Sensitive Detector	45

Figure No.	Title	Page
16	Front View of the Control Rack	47
17	Rear View of the Control Rack	48
18	Block Diagram of Field Stabilizer . . .	49
19	Schematic of the Integrator and Generator Regulator	51
20	The Resolving Slit Geometry	57
21	Two Views of the Helical Trajectory . .	59
22	The Three Instrumental Contributions to the Line Profile	63
23	The Instrumental Profile for a Disk Source	64
24	An Illustration of the Semi-Apex Angle Chosen for the Cone Source	66
25	The Profile for a Muller-Type Source	67
26	The Instrumental Profile for a Cone Source	69
27	An Experimentally Observed Profile with a Cone Source	72
28	A Coarse Search Run With a Thorium Source	74
29	The Resolution of the F and E_d Lines	76
30	The Leading Edge of the I Line as Observed Using a Cone Source	78
31	The Geometry and Nomenclature of the Square Coil Pairs	89
32	The Geometry and Nomenclature of the Double-Helmholz Sweep Coils	93

I. THE THEORY OF THE DESIGN OF THE SPECTROMETER

A. Introduction

The conditions affording optimum luminosity and resolution for an axial beta-ray spectrometer with uniform magnetic field were first developed by Professor DuMond[1]. His analysis was greatly simplified by the adoption of a uniform magnetic field as the basis for design, for the principles revealed by Professor DuMond could scarcely have been obtained with many types of field configurations commonly in use.

Since these design principles underlie the whole development which follows, and since cognizance of them is the natural introduction to the work reported herein, they will be outlined at this time.

It is commonly known that an electron follows a helical path as it moves through a uniform magnetic field. This motion and the coordinates necessary for describing it are shown in Figure 1. A straightforward calculation yields the following important relations among these coordinates:

$$y = R \sin\psi \qquad R = 2(p/Be)\sin\theta$$

$$x = (L/\pi)\psi \qquad L = 2\pi(p/Be)\cos\theta$$

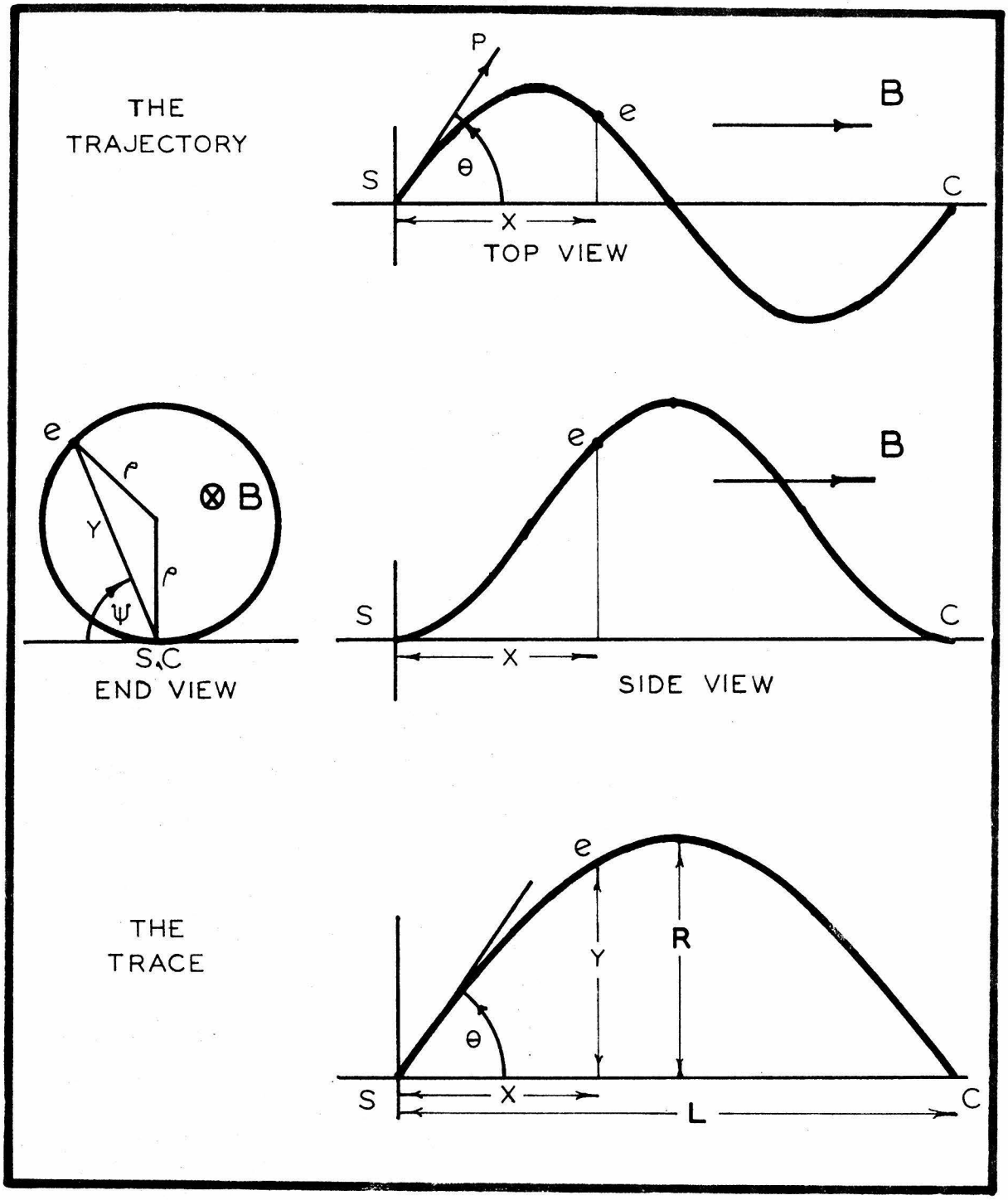

FIGURE 1. THE TRAJECTORY IN THREE VIEWS AND ITS TRACE.

If a quantity Q is chosen proportional to the total momentum, where $Q = 2(p/Be)$, y can be expressed as

$$y = (Q\sin\theta) \sin \frac{x}{Q\cos\theta} \quad . \qquad (2)$$

This is precisely the equation most useful for determining the optimum conditions of operation of an axial spectrometer. It characterizes the entire class of mono-energetic electrons leaving the point S at an angle θ with respect to the direction of the magnetic field.

Since in an axial spectrometer the trajectories have arbitrary azimuths initially, those described by Q and θ determine a cigar-shaped surface having cylindrical symmetry about the axis from S to C. The equation for y is therefore that of the curve seen in the plane cross-section of this surface through its axis. This curve, showing the radial displacement of particles from the axis as a function of displacement along it, is called the trace. It characterizes a particular group of particles described by Q and θ.

For the special case of a uniform magnetic field the equation of the trace is known. It is simply a sine function. Figure 1 also gives the trace of the helical trajectory shown there.

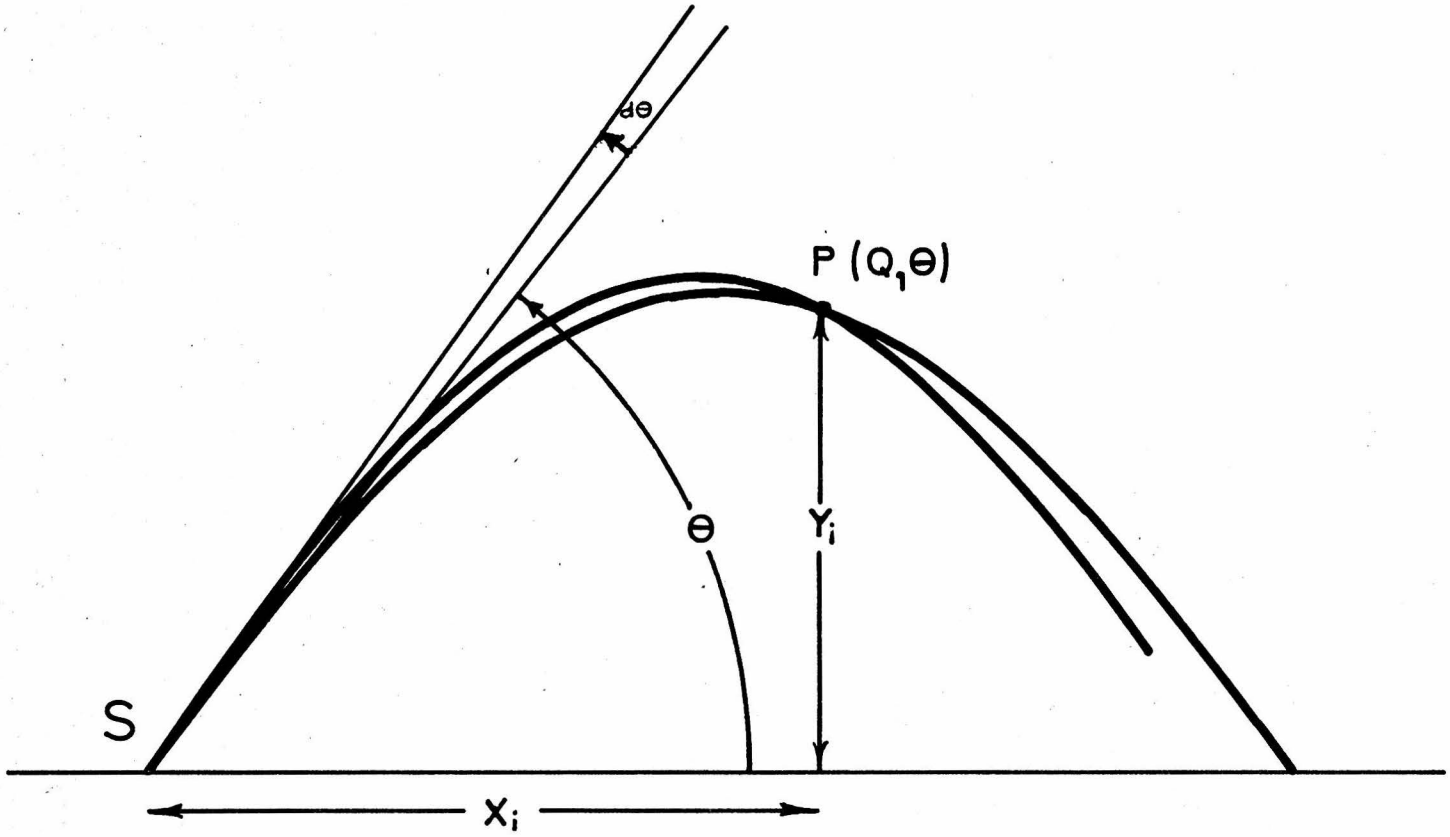

FIGURE 2 THE ULTIMATE INTERSECTION OF TWO COALESCING TRACES

B. The Determination of the Ultimate Intersection of Two Coalescing Traces.

Traces for two electrons that have the same Q but differ slightly in departure angle θ are shown in Figure 2. As they coalesce to the same θ, the two traces determine an ultimate intersection at a point $P = P(Q,\theta)$.

Following paragraphs will show that all other traces passing through P must have a greater Q than that of the trace at angle θ. This minimum Q at θ means that a resolving slit placed at the circle represented by P can select the largest fraction of the total sphere about the source at S for transmission with a specified inhomogeneity of momentum.

It is instructive to imagine the effect of a monoenergetic point source of particles at S. With such a source in place, all other traces (at angles either larger or smaller than θ) will pass nearest P inside that point. That is, their points of nearest approach to P will lie within the area enclosed by the trace for which P was determined.

Thus if a monoenergetic source is placed at S and the magnetic induction is increased, the number of traces enclosing P (consider a large but finite number of traces at various angles) will gradually decrease until the very

last trace to pass over P and miss the inner edge of the resolving slit will be the trace at angle θ. It is therefore called the ultimate trace.

The coordinates of the ultimate intersection of two traces that coalesce to a single trace described by Q_1 and θ_1 can be found from equation (2). They are

$$x_1 = (Q_1 \cos\theta_1)\psi_i \qquad (3)$$

$$y_i = (Q_1 \sin\theta_1)\sin\psi_i. \qquad (4)$$

Figure 1 shows that ψ_i is the azimuth of the intersection. It is found from the relation

$$\tan\psi_i/\psi_i = -\tan^2\theta_1. \qquad (5)$$

C. <u>The Determination of the Co-latitude Angle Optimizing the Luminosity for a Specified Resolution.</u>

Professor DuMond now showed that a θ_1 can be found which maximizes the luminosity that can be obtained with a specified inhomogeneity of momentum. That is, a value of θ_1 exists which maximizes the fraction of the total sphere about S that can be used for a specified inhomogeneity of momentum from the use of a finite solid angle. This optimum value for θ is found by substituting the coordinates of the ultimate intersection, equations (3) and (4), into the equation of the trace, (2), obtaining

$$\left(\frac{Q_1 \sin\theta_1}{Q\sin\theta}\right)\sin\psi_i = \sin\left(\frac{Q_1\cos\theta_1}{Q\cos\theta}\psi_i\right) \tag{6}$$

Parameters r and δ are defined as follows:

$$r = \frac{Q - Q_1}{Q_1} \ll 1 \tag{7}$$

$$\delta = \frac{\cos\theta - \cos\theta_1}{\cos\theta_1} \ll 1 \tag{8}$$

It is then a routine calculation to obtain the expressions,

$$\frac{Q_1 \sin\theta_1}{Q\sin\theta} = \left(1 + \frac{\delta}{\tan^2\theta_1} + \frac{1}{2}\frac{\delta^2}{\tan^2\theta_1} + \frac{3}{2}\frac{\delta^2}{\tan^4\theta_1} - r\right) \tag{9}$$

and

$$\frac{Q_1\cos\theta_1}{Q\cos\theta} = \left(1 - \delta + \delta^2 - r\right) \tag{10}$$

Terms in r^2 and δ^3 and higher are neglected. Substitution of these quantities into equation (6) results in the following equation:

$$r = (1/2)\left[3\cot^2\theta_1 + \psi_i^2\sin^2\theta_1\right]\delta^2. \ * \tag{11}$$

The definitions of Q and r show that r symbolizes a relative inhomogeneity of momentum.

---

*This equation differs slightly from the one originally given in reference 1. This is the result of a correction replacing 5/4 by 3/2 as the coefficient of $\delta 2/\tan^4\theta_1$ in equation (9). The correction is not of great importance however, for it brings the optimum θ even nearer the design value, 45°, than before.

If a quantity ϵ is chosen as the ratio of kinetic to rest energy for the particle, the three quantities, p, ϵ, and r are related by the equation:

$$\frac{\Delta\epsilon}{\epsilon} = \left(\frac{\epsilon+2}{\epsilon+1}\right)\frac{\Delta p}{p} \cong \left(\frac{\epsilon+2}{\epsilon+1}\right) r \qquad (12)$$

The expression for δ is related to the solid angle by showing that

$$\Phi = (1/2)\left|d(\cos\theta)\right|_{\theta_1} \cong (1/2)\left|\cos\theta_1 \delta\right| \qquad (13)$$

where Φ is the fraction of the total sphere from the source between cones of half angle θ_1 and $\theta_1+d\theta$. Due to the dependence of r on δ^2, this is only half the solid angle corresponding to a specified r. The use of the additional solid angle between θ_1 and $\theta_1-d\theta$ introduces no further inhomogeneity of momentum. Therefore, the fraction of the total sphere $\mathbf{\Phi} = 2\Phi$ can be used for a given r and equation (11) can be re-written as

$$r = (1/2)\left[3\csc^2\theta_1 + \Psi_i^2\tan^2\theta_1\right]\mathbf{\Phi}^2 \qquad (14)$$

It is evident that the desired value of θ_1 minimizes r for a given $\mathbf{\Phi}$. This θ_1 minimizes the bracketed expression of equation (14). It is found to be $45^\circ 23'$. However, the bracketed expression has little slope near the minimum

and changes but little in magnitude between 40° and 50°. Hence the convenient value of $\theta_1 = 45°$ was chosen for the design of the spectrometer.

D. <u>The Dimensions of the Ultimate Trace of the Spectrometer</u>

The focus at P is now easily found to occur at $\psi_i = 116°14.3'$ or 2.02875 radians for $\theta_1 = 45°$. The diameter selected for the inner edge of the resolving slit then fixes the remaining dimensions of the spectrometer as shown for the ultimate trace in Figure 3.

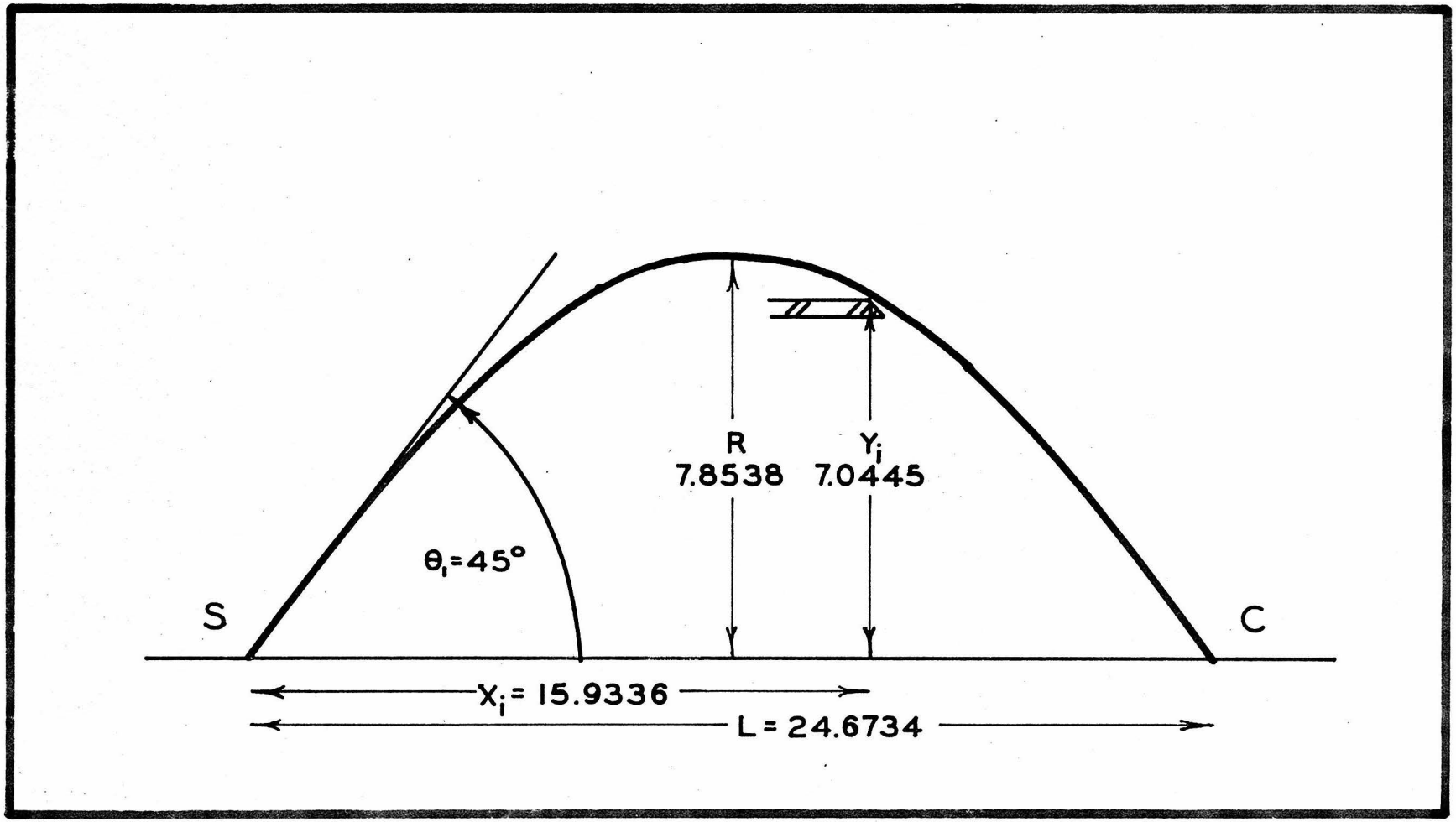

FIGURE 3. THE DIMENSIONS OF THE ULTIMATE TRACE IN INCHES.

II. THE CONSTRUCTION OF THE SPECTROMETER

A. The General Features of the Spectrometer.

The design of a beta-ray spectrometer realizing the optimum operating conditions outlined in the previous section was also conceived by Professor DuMond. His unique design is fully outlined in a report to the Research Corporation and the Office of Naval Research[2]. Only a few of the features bearing on the operational adjustments and the reproducibility of the measurements obtained with the instrument will be mentioned at this time.

A complete cross-section view of the spectrometer is given as Figure 4. The spectrometer field coils distribute their magnetomotive force uniformly along the major axis of a prolate ellipsoid. The mean radii of their turns conform to this surface of revolution. A very nearly homogeneous magnetic field is produced throughout the volume enclosed by the coils in this way.

Three operational adjustments can be made by control shafts projecting into the interior of the instrument through vacuum-tight "O"-ring seals.

An entrance aperture, the first defining slit encountered by the trajectory along its path from the source to the counter, can be adjusted with a calibrated drum dial to utilize radiation emanating from as much as 8.8% of the total sphere about the source.

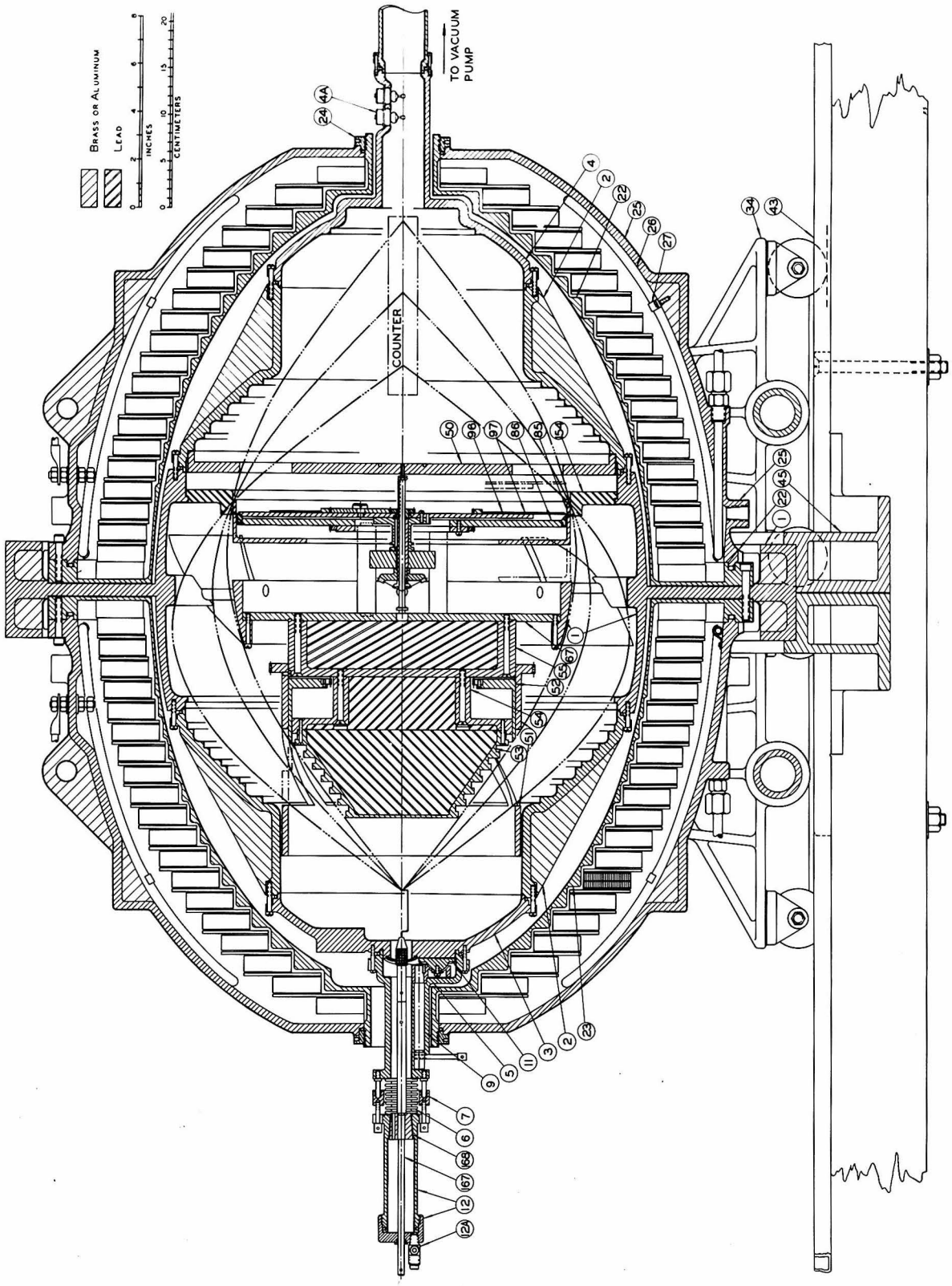

FIGURE 4. COMPLETE CROSS-SECTION VIEW OF THE HOMOGENEOUS MAGNETIC FIELD BETA-RAY SPECTROMETER.

A resolving slit having a maximum aperture of one-half inch (parallel to the axis) can be set with a micrometer dial calibrated in thousandths of an inch. The outer edge of the slit is fixed. The edge nearest the source (inside the ultimate trace) is moved by the dial. The position of this inner edge must be precisely known, for the position of the source is adjusted to correspond to it as shown in Figure 3.

It is also possible to move a retractable shutter into the path of the transmitted beam at a plane between the resolving slit and the counter. With the shutter extended to intercept the beam, particles from a selected azimuthal sector can be chosen for transmission. The shutter can select sectors of adjustable width as large as 180° in any azimuth.

A set of measurements at different azimuths using the same spectral line is used to detect misalignment of the source. Following paragraphs devoted to the source assembly will explain the method of making adjustments to place the center of the source on the axis of the instrument.

It is, of course, essential to have the direction of the total magnetic field coincide with the mechanical axis of the spectrometer. This is accomplished by using pairs of square "Helmholz-like" coils to cancel the components of

fields normal to the axis of the instrument. These coils are shown in the photograph of the assembled spectrometer, Figure 7. They are discussed at greater length in Appendix I.

B. The Source Assembly

Although one cannot view the source after it has been placed in the spectrometer, its position is precisely known.

The radioactive source is mounted on the end of an insertion-rod that is provided with a precisely-machined, coaxial, conical male plug.* The conical male plug seats in a matching conical female socket located in the portion of the source assembly that extends outside the main field coils. The position of this half of the source assembly can be adjusted with respect to the main frame of the spectrometer.**

Prior to operation of the spectrometer, the position of the socket is adjusted to bring the center of the source into coincidence with the axis of the instrument. The retractable shutter described earlier detects initial misalignment. Micrometer screws then move the socket relative to the rigid frame of the spectrometer to affect

---

*The rod and plug are shown as parts numbered 167 and 168 in the assembly drawing, Figure 4.
**The adjustable socket is part number 12 in Figure 4.

the desired alignment.*

The axial position of the conical socket (relative to the defining edge of the resolving slit) is also known by direct measurement.

The task of inserting a "calibrating" source (ejecting electrons converted by gamma radiation of precisely measured energy) and effecting its removal and the reinsertion of the "unknown" source at the same exact position is thus solved. It is sufficient simply to be assured that both of these sources are placed on the insertion rod at exactly the same position relative to its conical plug.

A jig for making this alignment is shown in Figure 5. It consists of an elbow microscope positioned with a micrometer screw by a drum dial calibrated in thousandths of an inch. A conically tapered female socket exactly matching that in the spectrometer is fixed in the bearing block shown opposite the microscope.

To align the source, the plug on the insertion-rod is first snugly seated in this socket. Three degrees of freedom then are available for adjusting the source position relative to the cone. A micrometer screw moves the brass

---

*The vacuum-tight sylphon bellows permitting this adjustment and the screws actuating it are parts numbered 6 and 7 in Figure 4.

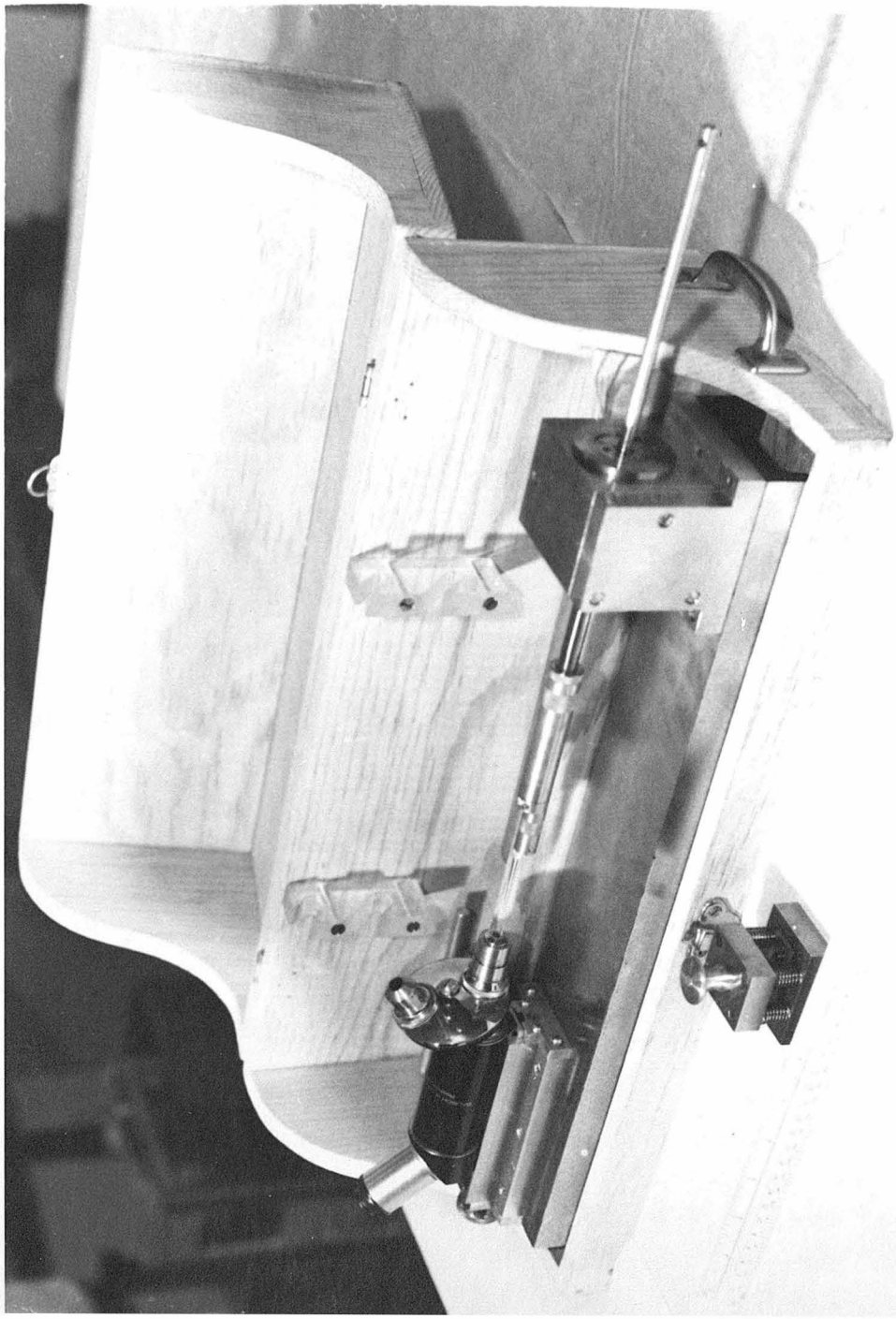

FIGURE 5. THE SOURCE-CENTERING JIG.

barrel at the end of the insertion rod to adjust the position of the source axially. Two additional adjustments are provided in the end mechanism to move the source radially.* The alignment is tested by rotating the insertion rod while keeping it snugly seated in the socket of the centering jig.

A discussion of source configurations is postponed for treatment in the section devoted to the line profile.

C. The Radiation Detector

The problem of obtaining a satisfactory radiation detector was solved by the construction of a thin-wall, cylindrical Geiger-counter tailored to fit the spectrometer. A photograph of the counter is shown as Figure 6.

Some 760 holes were drilled in the copper-plated brass tube forming the cathode. The holes enter the counter wall at an angle of 45° with respect to the counter axis, and the holes touch each other on the inner surface. This construction was adopted to obtain maximum transmission of the beta-radiation which is incident on the counter at this angle. It allows approximately 68% of the incident radiation penetrating the window to produce counts.

---

*One should note that Figure 5 shows the source holder actually used. This unit is unlike the one tenatively shown in the assembly drawing.

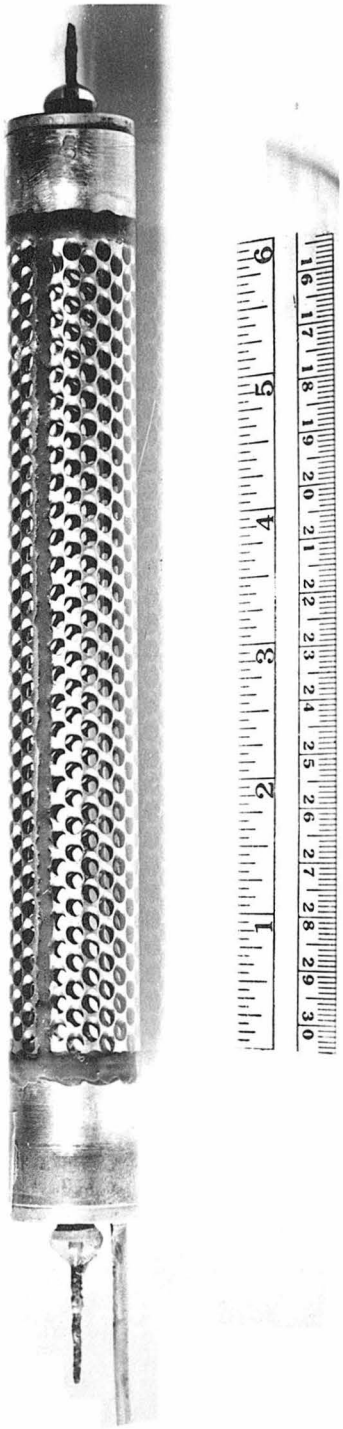

FIGURE 6. THE PERFORATED TUBE GEIGER-MULLER COUNTER.

The counter window was made of mica 0.0005 inches thick. This amounts to roughly 3.5 mg./cm.^{2} of mica. An excellent process for sealing the mica window to the tube was devised by Mr. Louis Bogart and is described in the report on the instrument(2).

A spring-loaded, one mil tungsten wire was used for the anode. A mixture of 7.5% ethyl alcohol in argon gave a 100 volt plateau with a slope of 5%.

The dead-time of the counter was measured by the "two-source" method. Five-minute runs with a peak counting rate in excess of 50,000. counts-per-minute gave a dead-time of 199.$\pm$1. microseconds. This dead-time would reduce the observed counting rate one percent at 3,000. counts-per-minute. Counting rates this large have never been used with the spectrometer.

The present counter is now the element that prevents the extension of the useful range of the spectrometer to lower energies. The author believes that counters of similar construction can be built with even thinner mica windows, and that flatter plateaus will be achieved by a leaner mixture of the alcohol quench. The possible adoption of a satisfactory scintillation counter may, of course, preclude this effort.

The assembled spectrometer is shown in Figure 7.

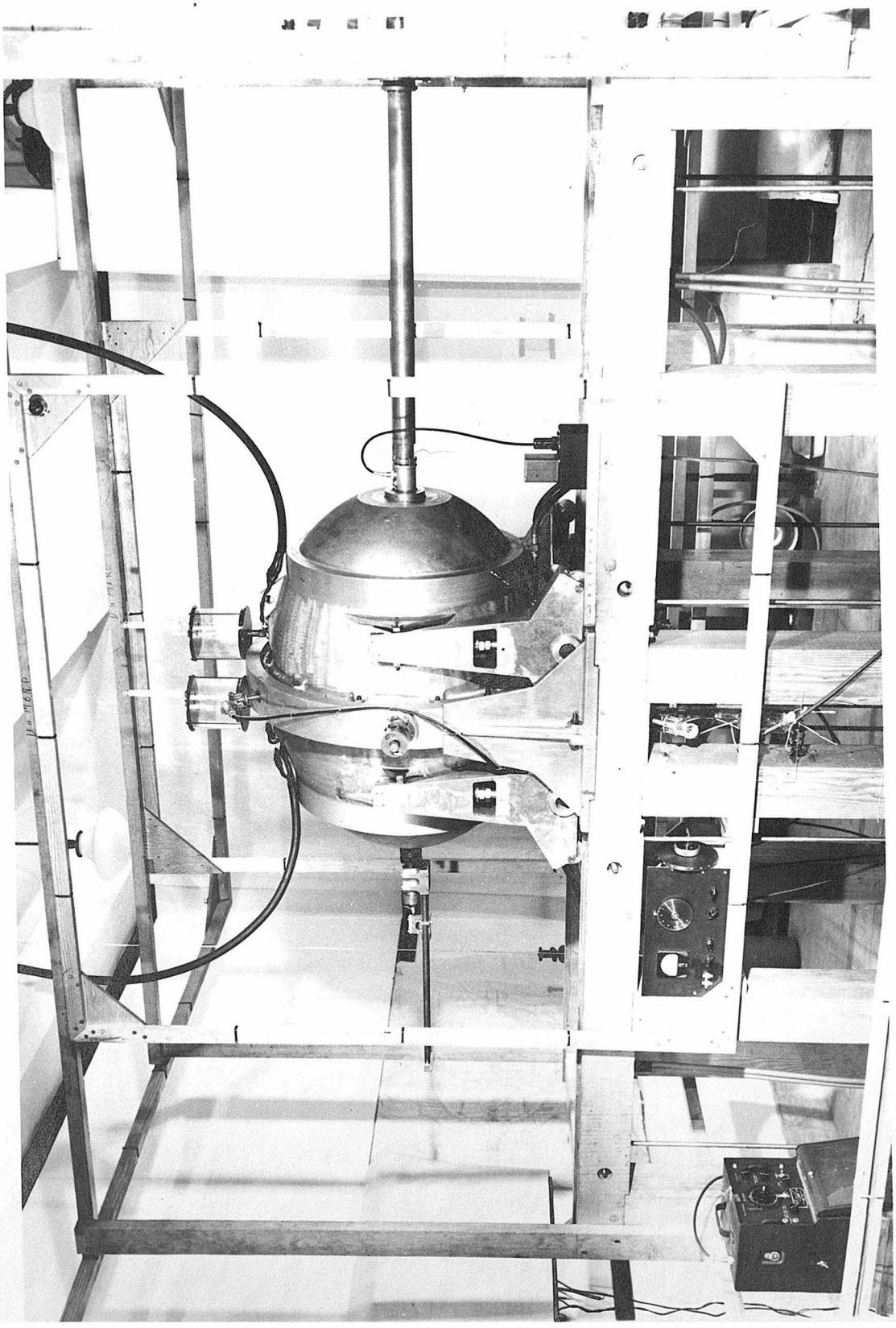

FIGURE 7. THE HOMOGENEOUS MAGNETIC FIELD BETA-RAY SPECTROMETER.

III. THE MEASUREMENT AND CONTROL OF THE MAGNETIC FIELD

A. The Operation of the Proton-Moment Circuit.

The ultimate precision of the measurements made with any magnetic beta-ray spectrometer certainly cannot exceed the accuracy with which the strength of the magnetic field is known. The most precise method of measurement and control known at the present time employs an effect of the unvarying magnetic moment of an elementary particle to obtain resonance signals for measurement and error signals for use in a servo system regulating the magnet current.

As early as the mid 1930's, experiments employing magnetic resonance techniques were used to determine the magnetic moments of the neutron and various nuclei. However, about ten years elapsed before the nuclear induction work initiated by Bloch(3) and the group at Stanford(4) led to an attempt to measure and control a magnetic field using signals obtained from protons immersed in the field(5).

The original induction method unfortunately required rather involved circuitry with critical adjustments at the r-f head where the proton sample was located. Hence it was unsuitable for the present application, since the type of system that could be employed with the spectrometer was in a large measure governed by the inaccessibility of circuit components required to be placed within its vacuum

envelope.

The simplicity achieved by using an absorption (rather than an induction) scheme was clearly necessary. The theoretical considerations involved in obtaining and interpreting nuclear absorption signals are extensively treated in an article published by Bloembergen, Purcell, and Pound[6]. The actual circuits designed to detect the absorption effect assume a variety of forms[6-10].

It is timely at this point to digress momentarily and review the considerations determining the compromise of design selected for a spectrometer.

A magnetic beta-ray spectrometer measures radiation in selected intervals in the beta-ray spectrum of a radioactive source by associating a value of $B\rho$ with them. Hence these two quantities are reciprocally related in a design compromise.

If ρ is made large, considerable ease of construction follows. Tolerances for machined parts can be relaxed, and the cost and delay of precision machine work is reduced. Slight deformities in critical parts diminish in importance. Furthermore, the size of the source is correspondingly larger, and its construction and precise installation are greatly simplified.

On the other hand, definite advantages accompany the choice of strong fields. Of course ρ is then made small, achieving economy as regards the cost of copper for field coils and other expensive material used for the construction of the spectrometer. The annoying effect of stray magnetic fields is also greatly reduced. Most important, strong magnetic fields are likely to result in the use of fields generally considered accessible for measurement with the proton moment.

The spectrometer size chosen by Professor DuMond was made large enough to insure that reasonable machine tolerances could achieve the desired mechanical precision. This resulted in the use of magnetic fields varying down to only 35 gauss. Ordinarily, the nuclear magnetic resonance absorption of the proton is detected at these weak fields only with considerable difficulty and by using very large proton samples.

One should realize at the outset that signal-to-noise ratios obtained with proton samples are inherently poor at such weak magnetic fields. Several alternatives are usually suggested.

The adoption of a paramagnetic resonance control scheme, known to produce strong signals with weak fields, would seem a natural alternative. However, the very considerable difficulties anticipated in adapting the high r-f frequen-

cies accompanying this method to the present application prohibited its use. Very limited access to the interior of the spectrometer (a necessary result of the design of the main field coils) demanded the use of wiring for connections and precluded any wave-guide installations.

Fortunately, the weakness of the proton signal is partially compensated for by the gain of a factor of from ten to one hundred in the sharpness of the resonance.

A study of circuits that could be adapted to the use of the proton method then followed. Since very poor signal-to-noise ratios were anticipated, circuits generating a complex spectrum of radio-frequency signals were not considered favorable choices. Such circuits, for example, might use frequency modulation to eliminate the usual "wobbling" or sweep coils. Others of the type include circuits using super-regenerative detection. This method obtains high sensitivity, but is one poorly adapted to control systems.

A circuit designed by Pound and Knight[10] best satisfies the requirements of our application in that it produces a driving r-f magnetic field of optimum intensity and of a single frequency. It is further ideally suited to a convenient control system in that its r-f oscillation is stabilized at the optimum level simultaneously for both sensitivity of the circuit and saturation of the proton sample. This is a great convenience in tuning.

It is indeed a pleasure to acknowledge our indebtedness to this original source, for the system we are now using is an adaption directly evolved from the original circuit of Pound and Knight[10].

In our adaptation of the circuit every effort was made to enhance the resonance signals and to reduce the noise entering low level stages of the oscillator. Some modifications of the original circuit were necessary to extend its operation to weak fields, and they will be noted in following sections.

A block diagram of the arrangement we are using is given as Figure 8. Its operation is briefly described as follows.

A constant-frequency r-f voltage is supplied to a coil surrounding a proton sample that is mounted within the main field of the spectrometer.

The strength of the magnetic field (of the spectrometer) is then brought to the value that causes the nuclear Larmor frequency of the protons in the field to equal the frequency of the r-f oscillator.* In the resonance condition protons in the sample absorb energy from the r-f source. In radio parlance, this changes the Q of the r-f coil and hence it changes the amplitude of the r-f oscillation.

---

*This occurs at 4.2578 kilocycles per gauss[11].

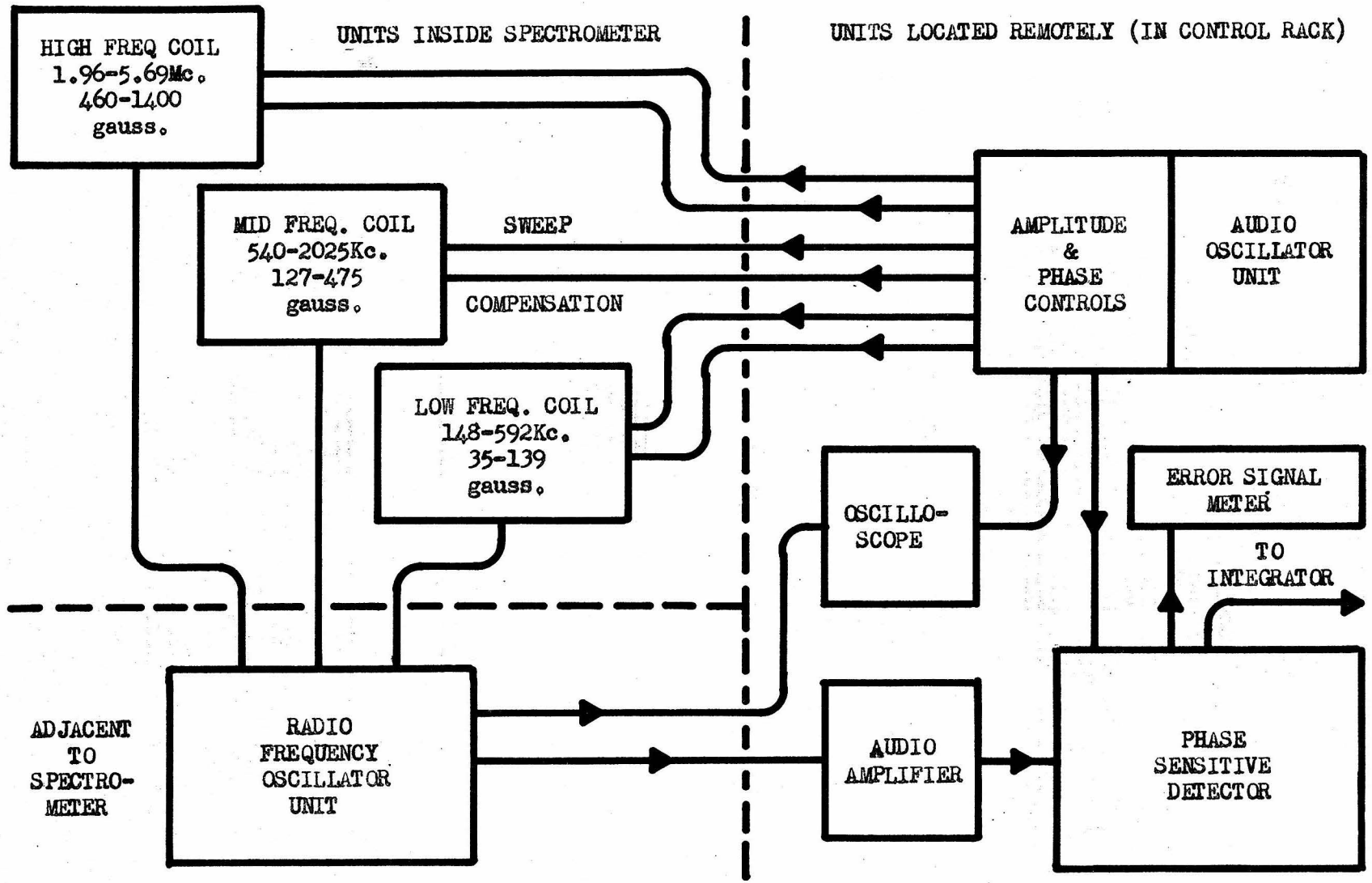

FIGURE 8 BLOCK DIAGRAM OF PROTON RESONANCE UNITS

An additional sweep magnetic field is then superimposed on the main field of the spectrometer. The sweep field is varied sinusoidally at an audio frequency with small amplitude. It therefore causes the amplitude of r-f oscillation to fluctuate each time the total magnetic field reaches the resonance value.

This fluctuating r-f level is amplified, demodulated, and the resulting audio signal is again amplified in the so-called r-f oscillator unit.

At this point the signal can be viewed as the vertical deflection of an oscilloscope trace. If a horizontal deflection is provided by the audio-frequency voltage supplying the sweep coils, the absorption curve is readily seen.

This signal is amplified further and sent to a phase sensitive detector where it is compared with the original audio sweep signal. The sweep-frequency component of the absorption signal changes 180° in phase as the peak of the resonance is crossed. The phase detector is thus able to produce an output voltage with amplitude and polarity corresponding to the magnitude and direction of the deviation from the resonance field.

If the sweep-field magnitude were made vanishingly small but not zero, and the spectrometer field were made to cross the resonance slowly, the phase detector would

produce the exact derivative of the absorption curve.

The error signal produced by the phase detector is suitable for control purposes, and it is used at the input of the field stabilizer and regulator.

The same error signal is also sent through a differential amplifier to a zero-center milliameter which shows the approximate derivative of the absorption curve. This signal is the most convenient one to use for aligning the equipment prior to use of the spectrometer.

1. The Resonance Heads

Both the limited space available in the interior of the spectrometer and the difficulty of obtaining access to the interior regions limited the number of resonance heads to three. It was therefore necessary to cover the entire range of magnetic fields from 35 to 1300 gauss with only three coil assemblies. This was managed by using each r-f coil for two overlapping ranges of frequency, an adjustment made in the r-f oscillator unit.

The construction of the largest of the three coil assemblies is shown as a scale drawing in Figure 9.

The outer forms (for the sweep coils) were turned from aluminum alloy stock and are precisely spaced by rods machined from brass. Plastic insulating inserts cast into slots cut into each of the forms reduce eddy currents.

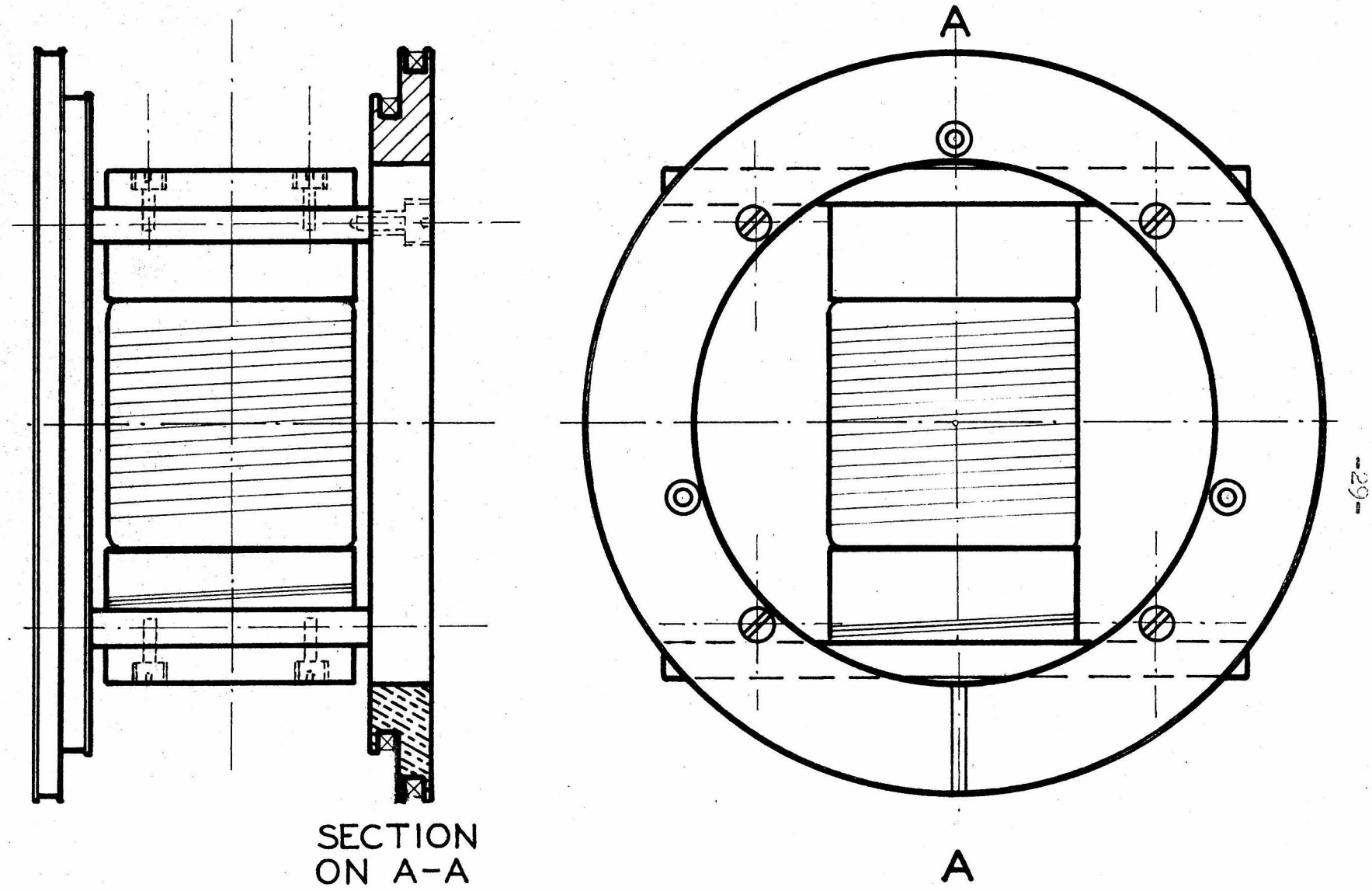

FIGURE 9 SCALE DRAWING OF THE LARGEST RESONANCE HEAD

They also provide space for bringing the coil connections to terminals.

Four spacing-rods support two Lucite plates for each coil set. The proton samples are held in hermetically-sealed cylindrical glass containers supported between the plates by short hollow Lucite cylinders. The radio-frequency coil is wound directly on the glass sample container.

A compensating coil is provided to nullify the small but unavoidable coupling between the sweep coils and the r-f coil. If this coupling were not removed it would be detected as a false error signal and would result in a slight difference between the desired and resulting spectrometer fields. This coil is visible at the bottom of the Lucite cylinder supporting the sample bottle.

Connections for <u>each</u> of the three coils assemblies are brought through the central casting of the spectrometer by three leads supported in one-half inch O.D. brass tubes. These tubes serve as the common ground connection for the three coils of each set. The three leads for each brass tube are spring-loaded and fixed in position by Lucite spacers.

a. <u>The Sweep Coils</u>

Particular care was required in the design of the sweep coils for this application. Their alternating

magnetic fields could not be allowed to affect either the homogeneity or the constancy of the spectrometer field near the trajectories of the beta-particles.

A convenient solution for the problem was produced by Professor Leverett Davis of this Institute. The result is accomplished by following a design for the sweep coils consisting of two opposing, coaxial pairs of Helmholz coils of different diameters. By adjusting their ampere-turns to cancel their dipole moments, very little external field appears. In fact, the dominant term in the expansion for the external magnetic field of the combination varies with the inverse seventh power of the distance from the center of the coils.

Figure 10 shows the variation of the magnetic field intensity along the axis of the coils. The calculations giving the results shown in Figure 10 are given in Appendix II.

b. The Radio Frequency Coil

In their article on nuclear magnetic resonance absorption, Bloembergen, Purcell, and Pound(6) clearly show the considerations involved in the design of the r-f coil and sample. With an r-f magnetic field of peak amplitude $2H_1$,*

*The factor of two appears because the field is decomposed into two circularly polarized components only one of which is effective.

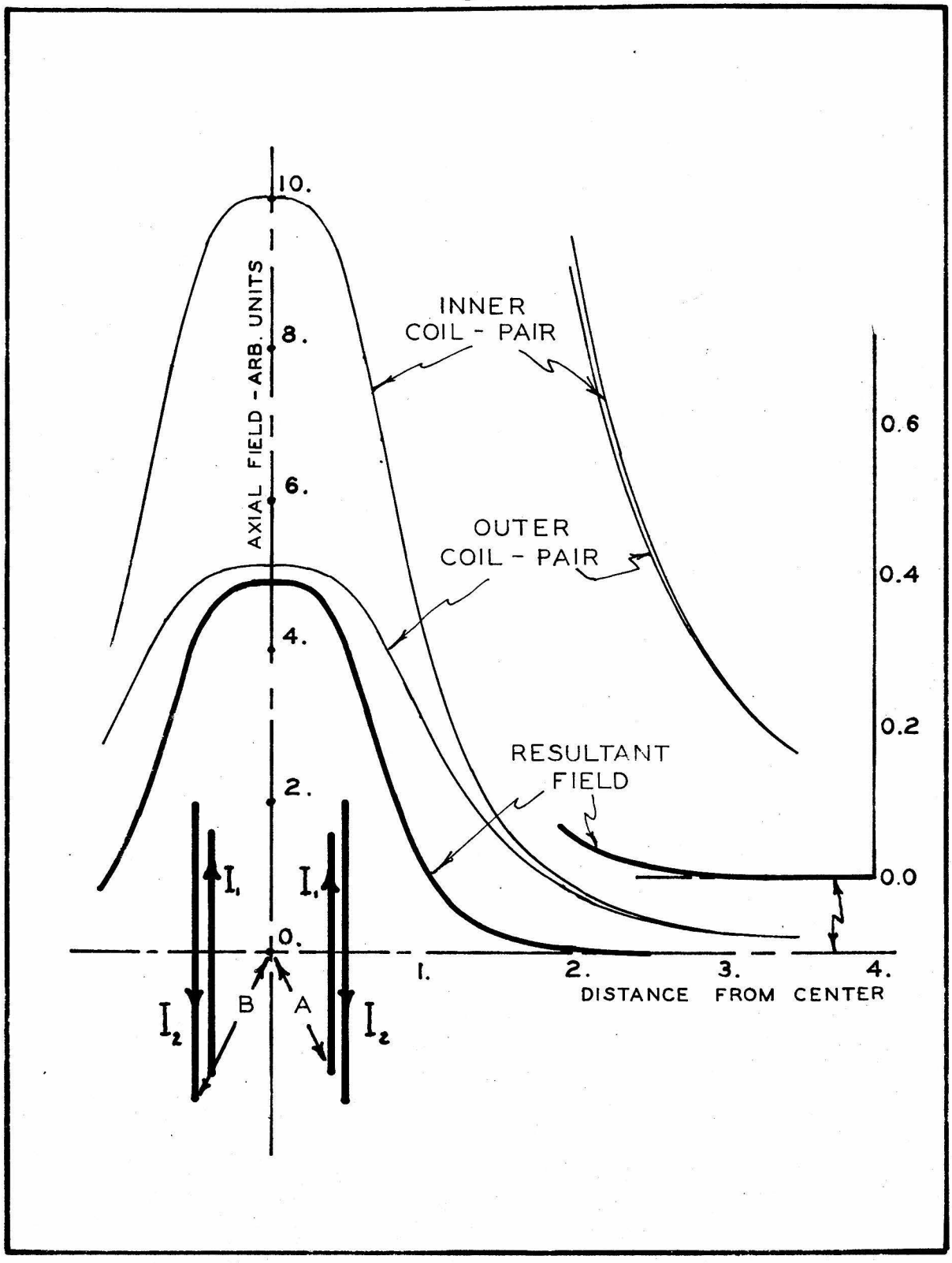

FIGURE 10. THE AXIAL VARIATION OF THE FIELD OF THE DOUBLE-HELMHOLZ SWEEP COILS.

they obtain an expression for P_a, the net rate at which energy is absorbed by the sample.* The expression for P_a is then interpreted in terms applicable to conventional circuit theory.

The symbol Q is used as a figure of merit for the inductances of circuit theory. It is most familiar when written as $\omega L/R$. In a more fundamental form, it can be written as

$$Q = 2\pi \frac{\text{Maximum energy stored in the field}}{\text{Energy absorbed per cycle}}. \quad (15)$$

The voltage across a parallel-resonant circuit using the coil is then directly proportional to its Q.

The authors[6] then use this definition of Q to obtain the relation:

$$\zeta\delta = 2\pi\left(\frac{(2H_1)^2/8\pi\zeta}{P_a/\nu_0}\right)^{-1} = \frac{\zeta P_a}{\nu_0 H_1^2}$$
$$= \zeta\left(\gamma^2\hbar^2 N_0 I(I+1)\nu_0 T_2^*/3kT\right) . \quad (16)$$

---

*The sample contains N_0 nuclei with spin I per unit volume. Its absolute temperature is T, and the Larmor frequency is ν_0.

In formula (16) ς is defined as a "filling" factor that relates the energy density in the field to the total energy that is stored in the field within the sample. T_2^* is a measure of line broadening; γ, h, and k are the gyromagnetic ratio and the constants of Planck and Boltzmann.

Since the energy absorbed by the proton sample and the coil are additive as far as the r-f oscillator is concerned, it follows that

$$\frac{1}{Q_r} = \frac{1}{Q_o} + \varsigma \delta \qquad (17)$$

Q_o is the Q obtaining at fields distant from the resonance. Q_r is the effective Q of the coil at the resonance value of magnetic field.

Since the energy absorbed by the sample is much less than that absorbed by the coil, equation (17) can be written approximately as

$$Q_r = Q_o(1 - \varsigma \delta Q_o) \qquad (18)$$

It is now evident that any feature of design increasing the magnitude of the term $(\varsigma \delta Q_o)$ will enhance the signals observed, for it will render the relative r-f oscillation level changes greater.

ς is improved by increasing the "coupling" between the sample and the coil. Experimentally, it was observed that

a solenoidal type of coil seemed to be more effective than a flat one, which would have had a higher Q. The factor was also increased by winding the coil directly on the sample bottle as close to the absorbing substance as possible.

Considerable effort was spent in producing a high-Q coil. The critical, low-frequency coil (Figure 9) was wound along a cylinder slightly longer than its diameter, since this was found to be the most effective as well as the most convenient shape of sample bottle. B&S No.33 Formvar-insulated copper wire was wound as a single layer coil having turns spaced about a wire diameter apart.*

without doubt, a larger coil would have had a better Q. Unfortunately, however, the size of the sample would have been enlarged in proportion (to keep ζ large) and this increase of sample size was not possible. The maximum size of the largest proton sample was limited by the space available for its sweep coils. The magnetic field of the largest set of sweep coils our available space would accommodate was not sufficiently homogeneous over a sample volume greater than 70 cc. Fortunately, with a homogeneous

---

*Litz wire, often preferred for coils operating in this range of radio frequencies, was found to afford no significant improvement in Q.

field spectrometer, it is not the main field that is the limiting factor in this regard.

The factors of δ were chosen the following way. T_2^* was largely fixed by the use of a 0.01 molar $MnSO_4$ sample.* This concentration was selected by experimentally observing the strength and sharpness of the signals obtained. A slight improvement might be had by finding a substance with a higher population of participating nuclei, N_o. Convenience led to the use of a water sample.

2. The Radio-Frequency Oscillator Unit

The construction of this unit is shown in photographs, Figures 11 and 12. The schematic diagram of the circuit is given as Figure 13.

A comparison with the original circuit[10] will show relatively few changes.

Six tuning ranges were adapted to three oscillator coils as shown in the schematic.

The use of a lower audio frequency sweep naturally resulted in decoupling and by-pass circuits appropriate for its use.

The known 0.01 molar $MnSO_4$ sample no longer required the original two second feedback time-constant for the

---

*Strictly speaking, the addition of paramagnetic ions reduces the spin-lattice relaxation time, T_1. However, T_2^* was defined to include all sources of line broadening.

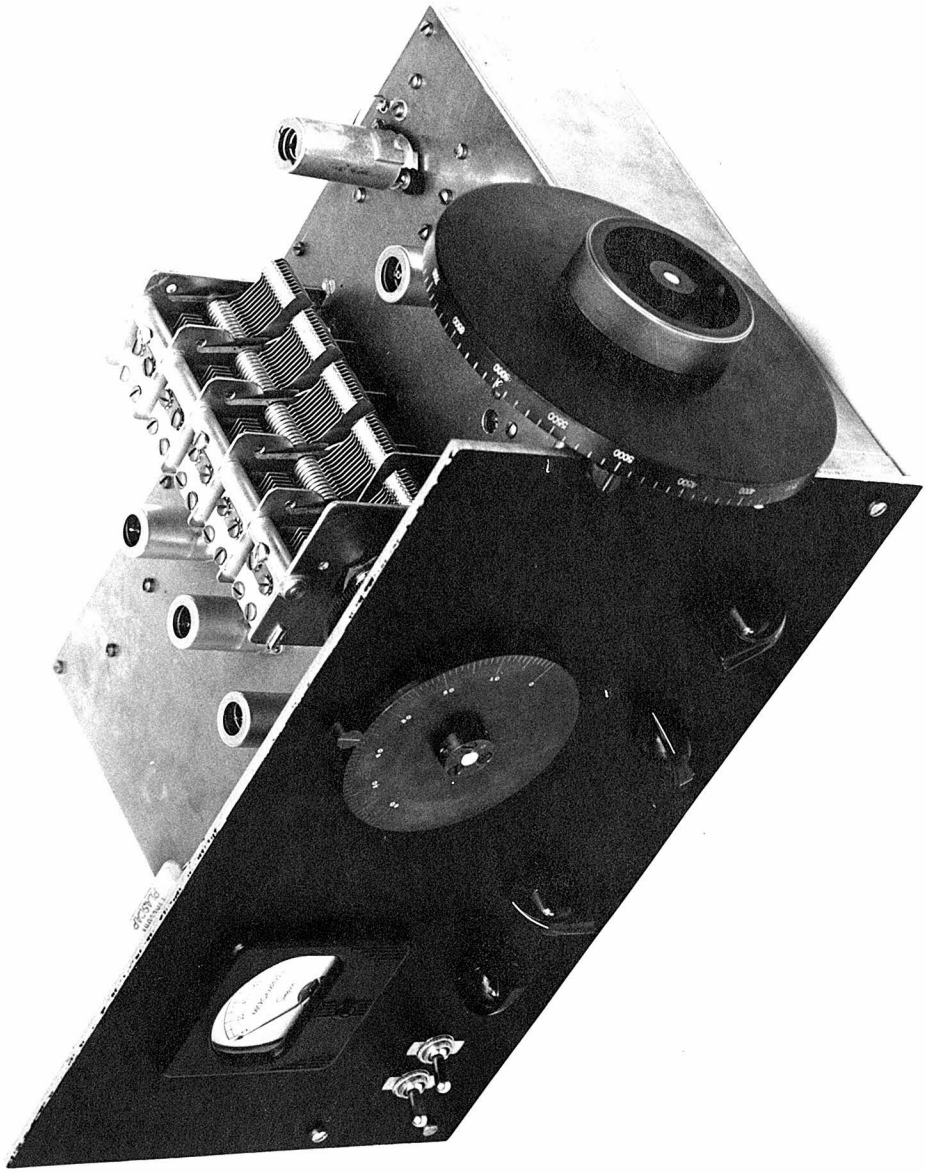

FIGURE 11. TOP VIEW OF THE PROTON RESONANCE OSCILLATOR.

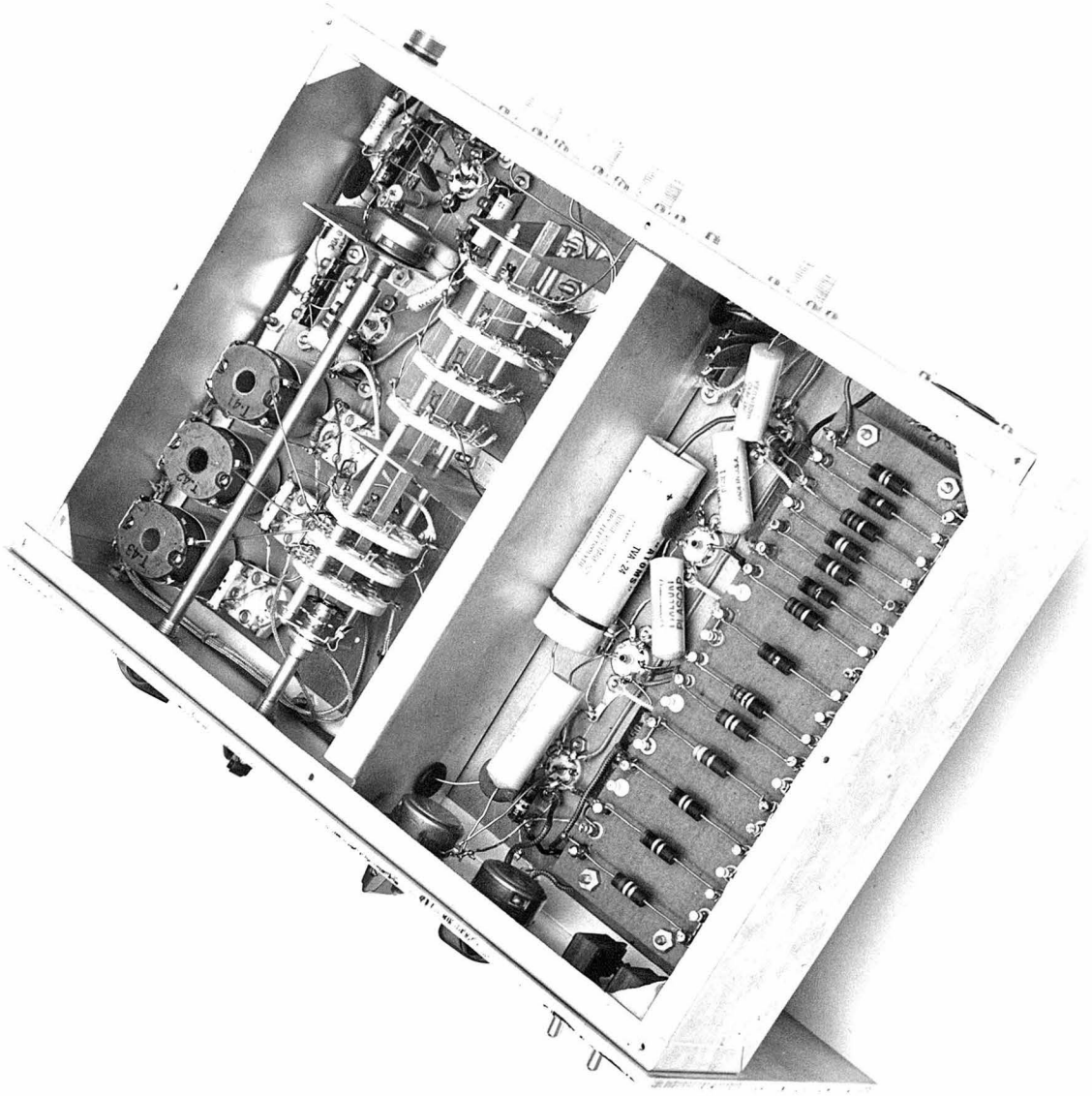

FIGURE 12. BOTTOM VIEW OF THE PROTON RESONANCE OSCILLATOR.

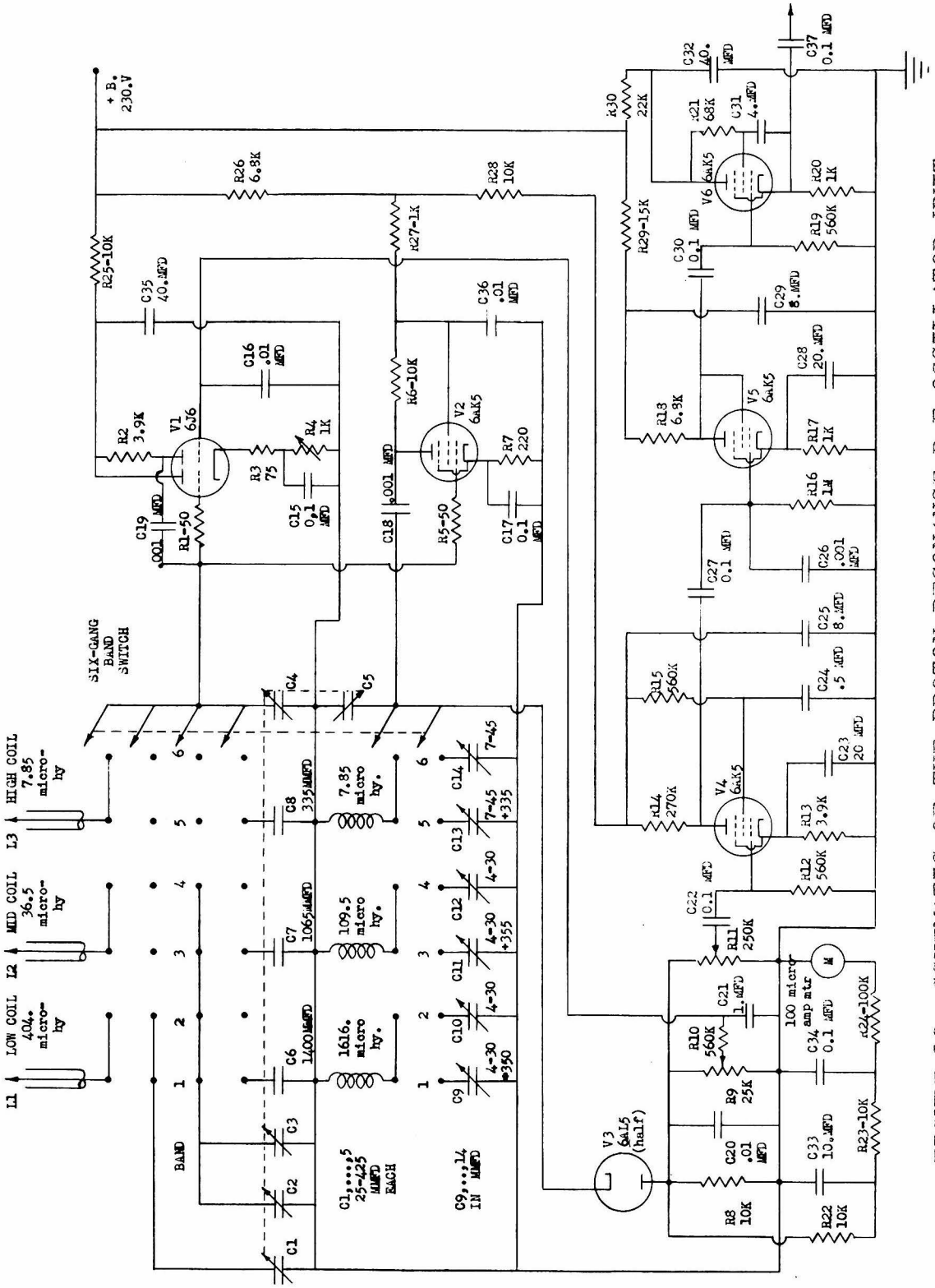

FIGURE 13. SCHEMATIC OF THE PROTON RESONANCE R-F OSCILLATOR UNIT.

oscillation level control. Therefore, this time-constant was reduced (at R10) by a factor of four. This reduction hastened the response of the oscillator to the slower r-f amplitude variations. This allows more rapid tuning and decreases the sensitivity of the oscillator tube to microphonics.

A more satisfactory detector, V3, was inserted and a standard pentode cathode follower, V6, was added at the output.

Since considerable effort was expended in achieving adequate signal-to-noise ratios with this equipment, a few remarks concerning design features found to be necessary and some typical difficulties encountered seem in order.

Every known precaution was used in the construction of the oscillator unit to prevent the entry of spurious signals, i.e., noise, in its low level stages. A preliminary test unit revealed the need for many precautions that would not have been considered otherwise.

A very irritating sort of noise enters as a 60 cycle signal from the 110 volt power distribution system. This noise enters each and every element where it is possible for it to creep in. For this reason, both a storage battery for the filament supply and a well-regulated power supply for the other circuit voltages are mandatory. Furthermore, a considerable improvement is obtained if the

power supplies are kept distant from all the circuits they supply. This separation was imperative in the cases of both the oscillator unit and the audio sweep generator.

The following unexpected effect was observed during the construction of the equipment. A noise of definite character was seen on the oscilloscope, and it was identified with a fundamental frequency of 180 cycles per second. By disconnecting cables, removing tubes, and the like, it was not difficult to trace its origin to a power transformer on the audio oscillator chassis (sweep frequency generator). The transformer was coupled magnetically to an output transformer supplying the sweep coils. This allowed the third harmonic of the power frequency to leak the full width of a chassis into a transformer core mounted ostensibly at right angles. The 180 cycle signal was picked up from the sweep coils inside the spectrometer and it was sent back through the r-f circuit and detected. The annoying coupling was eliminated by the isolation of power supplies in the present system.

Another type of interference was detected as extremely strong, sharp signals found at isolated points in the oscillator tuning range. Since very weak proton signals were evident, and "grass" or noise was being observed on the oscilloscope for removable noise components, the strong, isolated signals remained unidentified for a few days.

As soon as earphones were connected to the output of the oscillator unit, the voice of a popular singer, Bing Crosby, blared forth. The meticulously well-shielded circuit located within a steel building proved at least as sensitive to all nearby radio transmitters as most commercial radio receivers. Greater care in shielding in the present system removed the more harmful effects from this source. They are still observed with weak amplitude, and it is the author's belief that they will be found with any circuits of this type of useful sensitivity.

Since the various units of the system are distributed around the spectrometer room and in a generator room two floors below, great care was used to provide each unit with a single effective ground connection, and to insure that no other ground connections were inadvertently made. All the units located in the control rack were built without chassis grounds. This was done to prevent ground "loops" which would otherwise result from connections between units through the control rack.

The performance of the present r-f oscillator unit has been very satisfactory.

The amplitude of the driving r-f magnetic field was checked by using a vacuum tube voltmeter at the variable tuning-condenser to determine the average energy stored in the coil. It was found to correspond closely to the

optimum value.

The signals obtained with the present unit are observable as deflections of an oscilloscope trace at fields of only 35 gauss. With the narrow bandwidth inherent in the integrating circuit of the regulator they can be used for control when they cannot even be seen on the oscilloscope.

The frequencies corresponding to oscillator dial divisions vary about a percent from day to day. However, the use of selected, high-quality components and a high-Q coil make the oscillator frequency exceptionally stable during operation. This is the important requirement, since the frequency is always measured at each dial setting while the spectrometer is being operated.

3. The Audio Oscillator and Phase Sensitive Detector

Both of these units were built along very standard lines and need little description.

The audio oscillator that is used to supply sweep-frequency voltages to four different circuits is of the resistance-capacitance-tuned type with amplitude stabilization provided by inverse feedback[12]. It was designed to generate audio-frequency voltages over a single range from 30 to 300 cycles per second.

Provisions were made at each of its four output circuits for supplying the sweep voltages to the various units

with variable phase and amplitude. A simple and convenient circuit providing independently both amplitude and phase control with a possible variation of phase over 180° is shown as Figure 14.

The schematic diagram for the phase-sensitive detector is shown in Figure 15. It was built by Mr. James L. Kohl. Numerous published articles(13) describe circuits of this type.

No circuits having the narrow band-width ordinarily used for optimizing signal-to-noise ratios have yet been shown. In this system they are located in two places.

A variable R-C circuit is placed at the input to the differential amplifier. It provides a time-constant as large as several seconds for noise discrimination at the error signal meter.

If the error signal meter is observed with a very long time-constant before the main spectrometer field is turned on, a precise null in the pickup of the sweep signal by the r-f coil can be obtained. This is accomplished by adjusting the excitation of the compensating coil located in the resonance head. If the adjustment were not made, a small constant error would occur between the actual magnetic field and the spectrometer field demanded by the r-f oscillator unit.

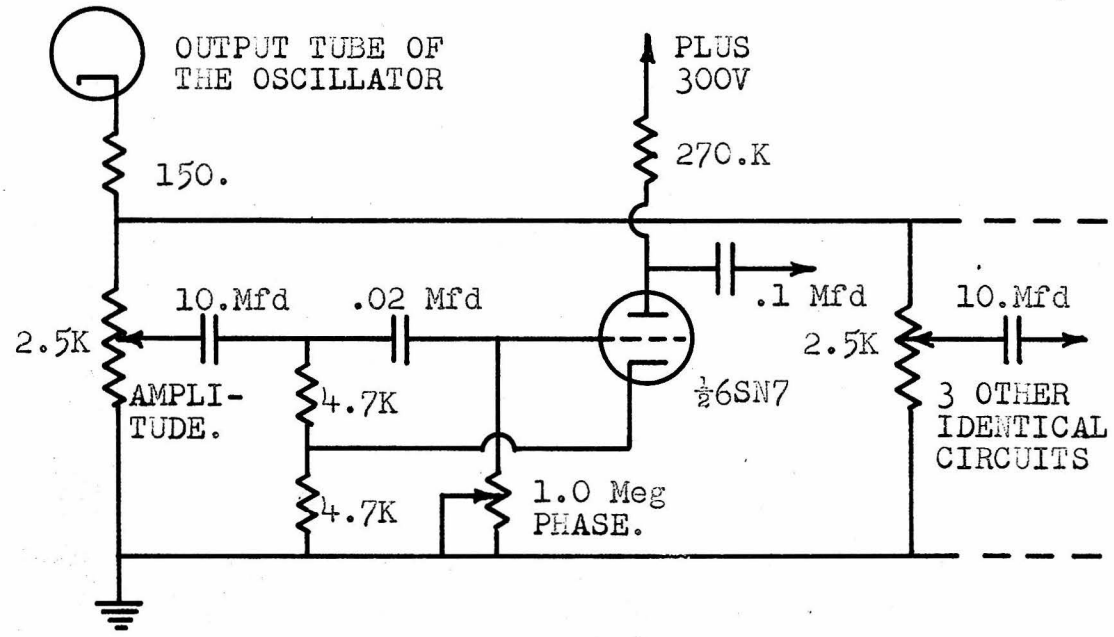

FIGURE 14 SCHEMATIC OF PHASE AND AMPLITUDE CONTROLS FOR THE AUDIO OSCILLATOR

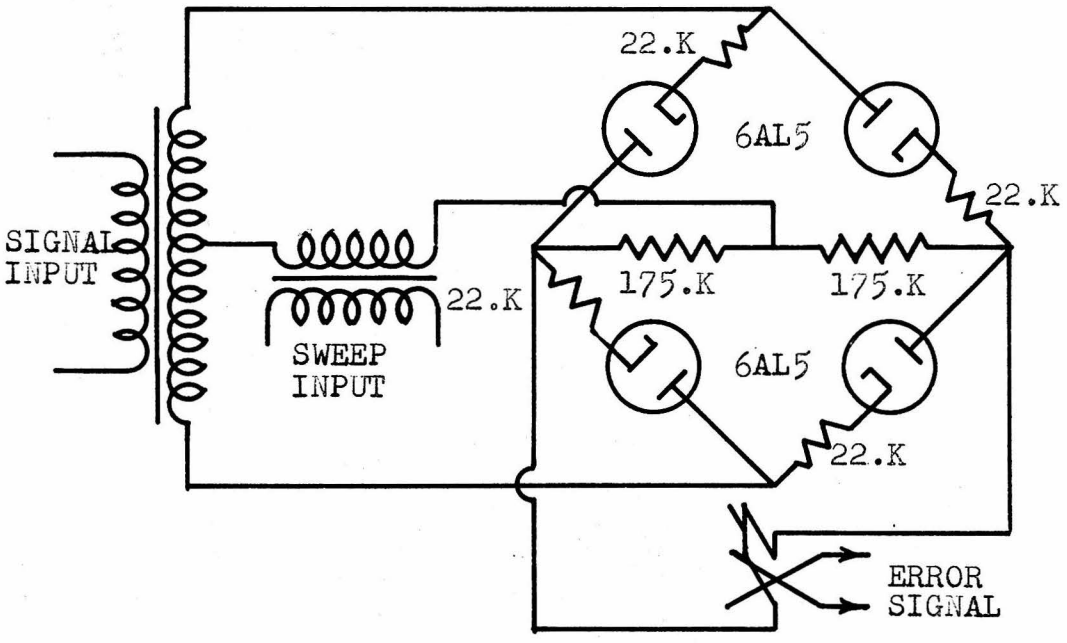

FIGURE 15 SCHEMATIC OF THE PHASE SENSITIVE DETECTOR

The narrow band width for the field regulator is provided in its first unit by an integrator having a huge time constant.

Photographs of the control rack that houses both these units and those of the regulator are shown as Figures 16 and 17.

B. The Magnetic Field Regulator

The units comprising this essential part of the system are the product of the considerable effort and ingenuity of Mr. James L. Kohl, who constructed them while the author was assembling the proton-moment field-measuring equipment.

A functional block diagram of the unit is given in Figure 18. Most of the units of the diagram are shown in photographs as Figures 16 and 17. The method of design employed follows that of Sommers, Weiss, and Halpern[14]. It converts a 35 kilowatt, 250 volt D.C. generator into a precisely controllable power source with low noise output. The details of construction will not be given here since they are fully described in a recent report to the Research Corporation and the Office of Naval Research[2].

The block diagram will show that the regulator and proton-resonance circuits are incorporated into a two-loop servo system.

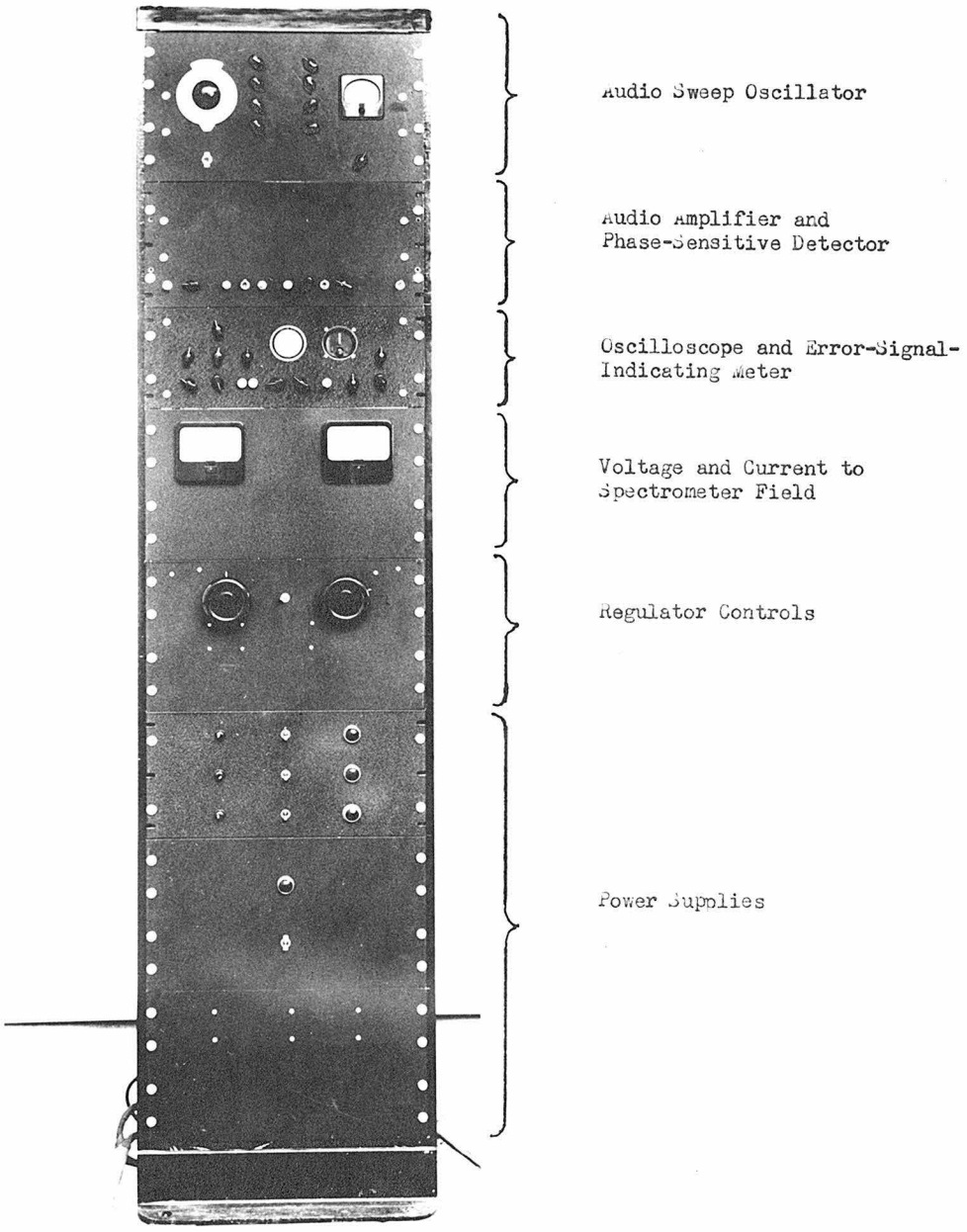

FIGURE 16. FRONT VIEW OF THE CONTROL RACK.

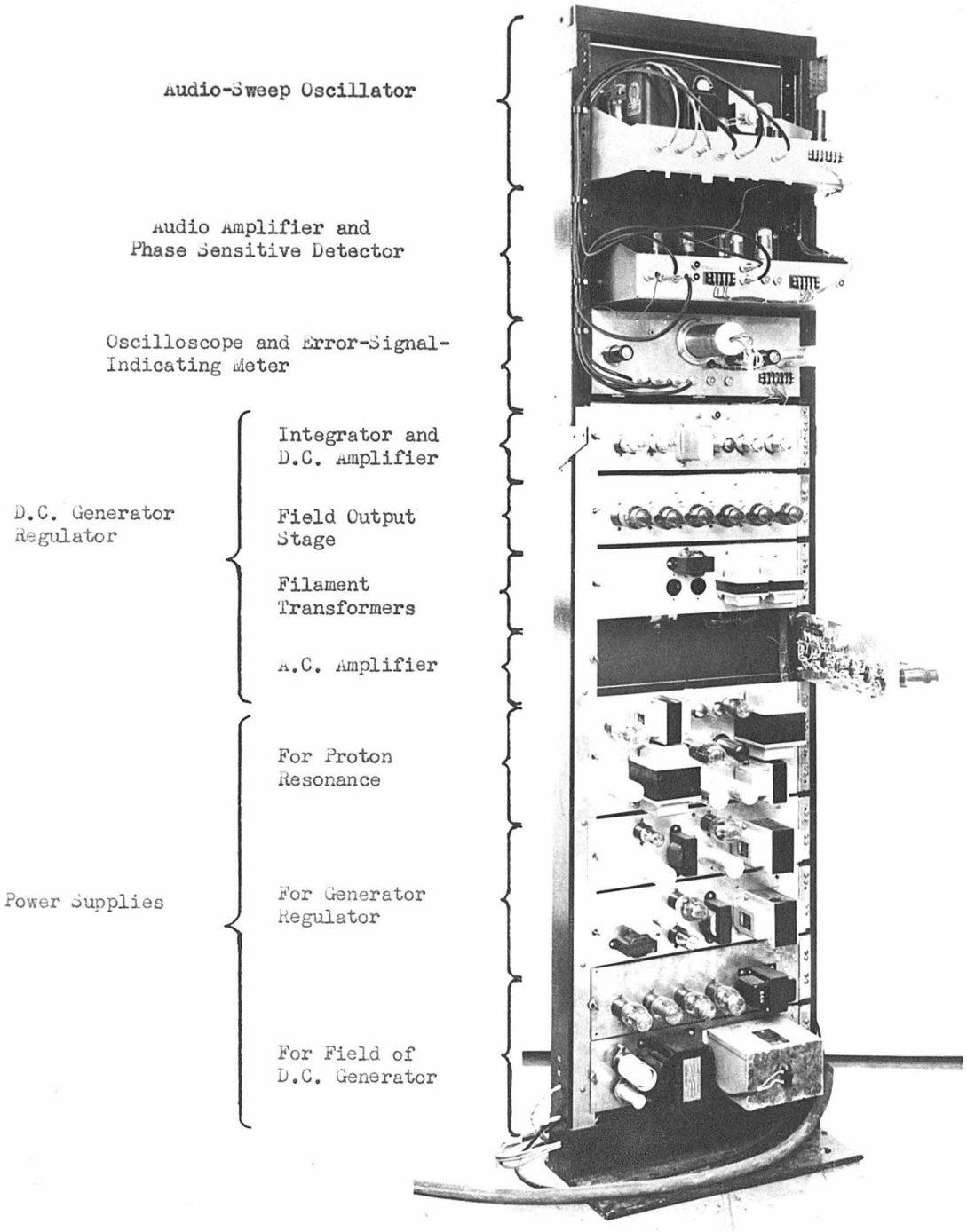

FIGURE 17. REAR VIEW OF THE CONTROL RACK.

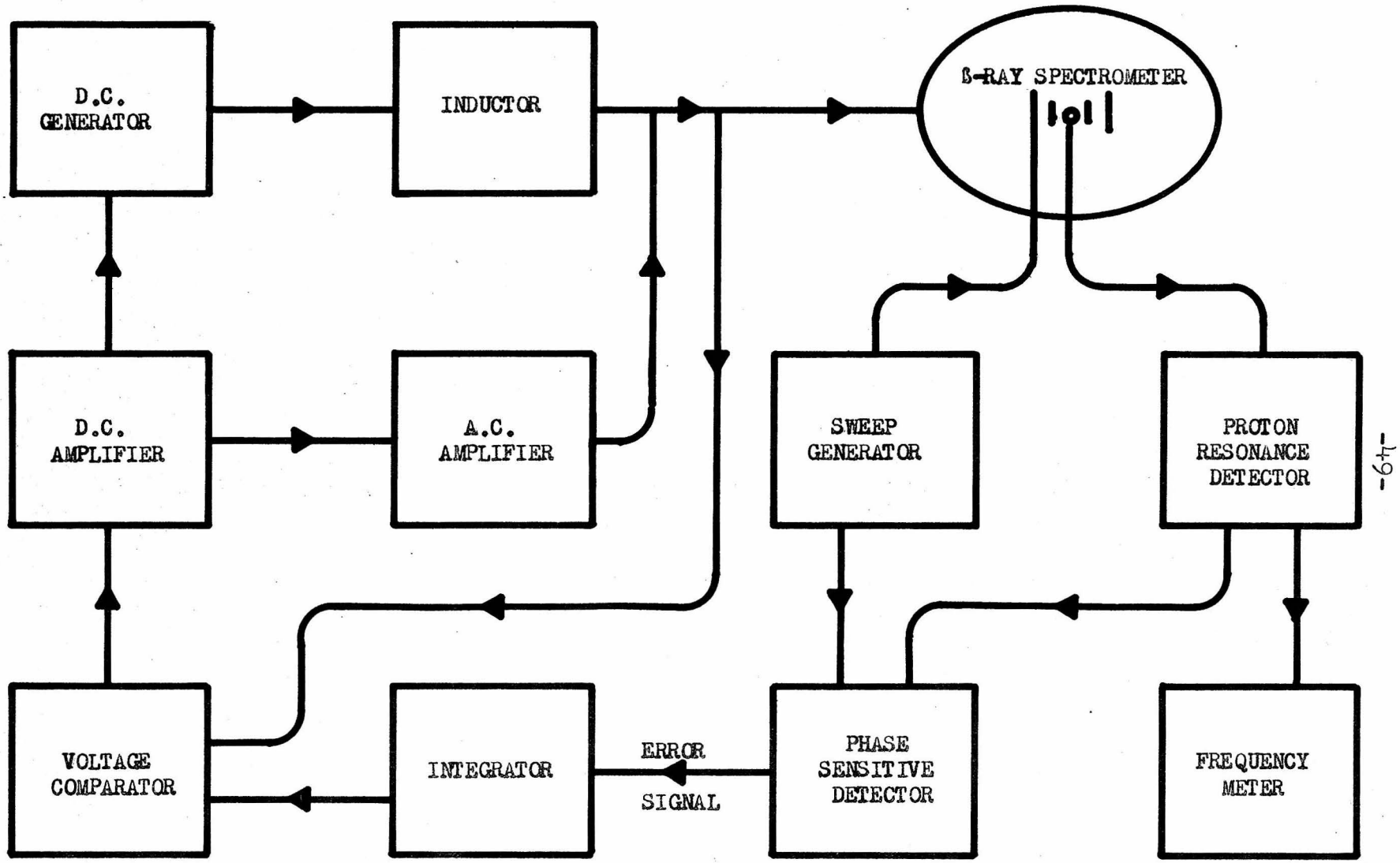

FIGURE 18 BLOCK DIAGRAM OF FIELD STABILIZER

One feedback loop serves to provide the separately excited generator field with D.C. excitation for smoothing out low-frequency surges. It also provides A.C. voltages nullifying the commutator hash from the generator.

The second feedback loop includes the proton resonance circuits. It provides the error signal that corrects the current supplied the spectrometer, maintaining the resonance between the proton Larmor frequency and the frequency of the r-f oscillator.

A very precise control of the spectrometer field is obtained in this way. With poor conditions that are present when high local noise levels obscure weak proton signals, the spectrometer current is stabilized to within 0.01% of the current desired. With more favorable conditions, a current stabilization of 0.002% is normally achieved.

Arguments have been advanced to the effect that the aluminum shell of the spectrometer conducts eddy currents making the actual field fluctuations much smaller than the coil current changes. In any event, however, the relative variations in the current are an upper limit to the relative variations of the magnetic field.

For reference, Mr. Kohl's circuit is given as Figure 19. It will be noted that it has been reduced in complexity

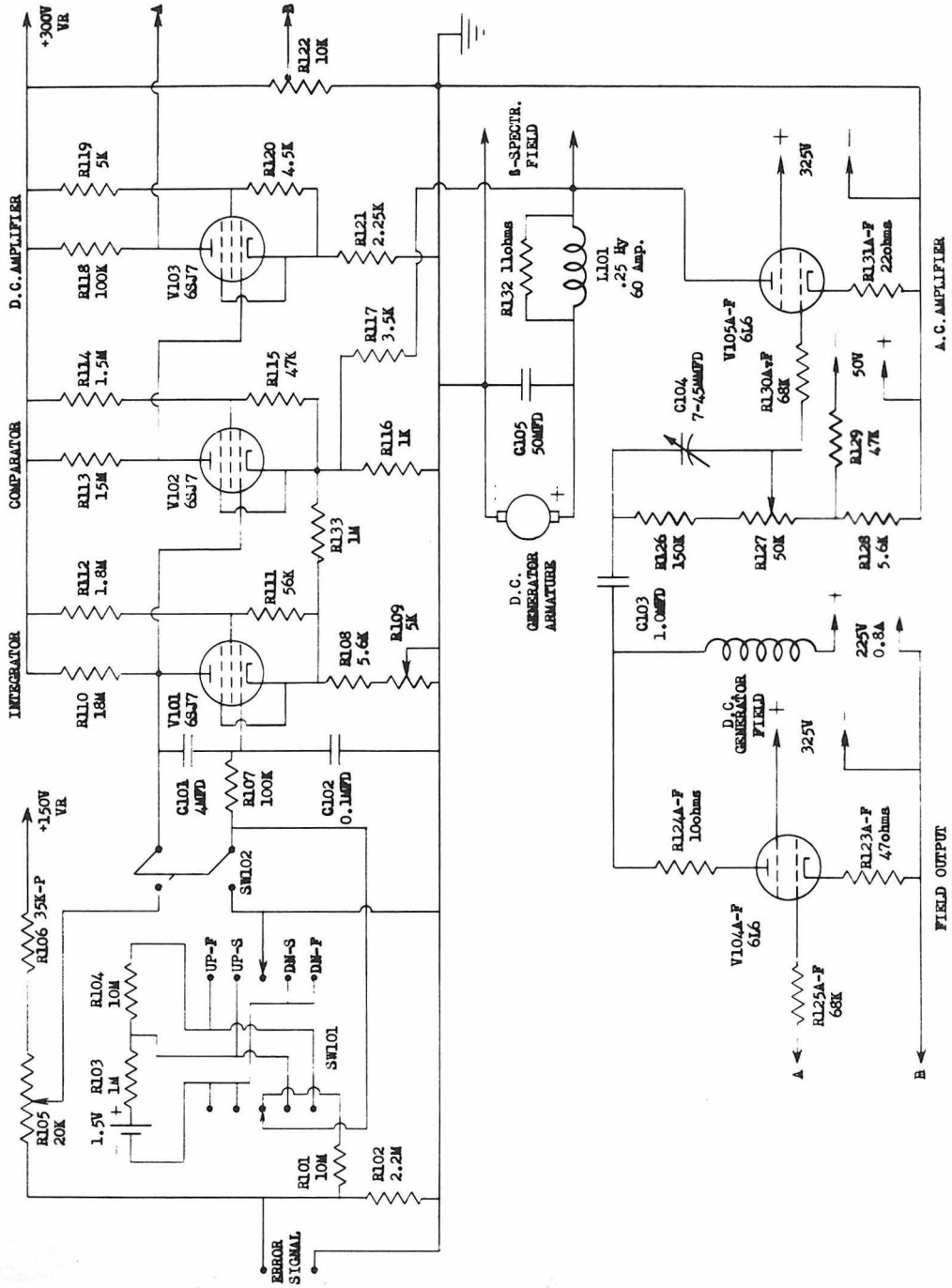

FIGURE 19. SCHEMATIC OF THE INTEGRATOR AND GENERATOR REGULATOR.

by representing groups of tubes having the same function as a single tube.

IV. THE LINE PROFILE

A. Instrumental Contributions to the Observed Line Width

Another great advantage of the homogeneous magnetic field is that it allows the calculation of the individual instrumental contributions to the broadening of the spectral lines observed with the spectrometer. Professor DuMond's analysis of these contributions(1) will now be outlined to show the procedure followed in adjusting the spectrometer for operation.

1. The Effect of a Finite Entrance Aperture

By considering a monoenergetic point source and an infinitesimally wide resolving slit, the effect of a finite entrance aperture can be revealed as follows. Equations

$$\frac{\Delta\epsilon}{\epsilon} = \left(\frac{\epsilon+2}{\epsilon+1}\right)\frac{\Delta p}{p} = \left(\frac{\epsilon+2}{\epsilon+1}\right)r \tag{12}$$

and

$$r = (1/2)\left[3\csc^2\theta_1+\psi_1^2\tan^2\theta_1\right]\Phi^{2*} \tag{14}$$

were derived in Section I. It was also shown there that the solid angle, Φ, is given by:

$$\Phi = 2\phi = \left|\cos\theta - \cos\theta_1\right| \tag{13}$$

---

*θ_1 and ψ_1 were chosen earlier as 45° and 2.02875 radians, respectively

If the solid angle is kept reasonably small, equation (14) can be written in a simpler form as

$$(\epsilon - \epsilon_1) = k\Phi^2, \tag{19}$$

where k is a constant. ϵ is the <u>apparent</u> ratio of kinetic to rest energy for particles emanating from the (monoenergetic) source at the angle θ that defines Φ. Particles confined to the ultimate trace have an energy corresponding to ϵ_1.

Since the counting rate is directly proportional to the solid angle used, equation (19) yields the relation:

$$\Delta N/\Delta\epsilon = C_1 \Delta\Phi/\Delta\epsilon = C_2/(\epsilon - \epsilon_1)^{\frac{1}{2}} \tag{20}$$

In other words, the profile due to the entrance aperture is infinite at ϵ_1 and it slopes toward lower energies with the inverse square root of $(\epsilon - \epsilon_1)$. However, this profile encloses a finite area in agreement with the transmission of a finite number of particles.

The width of the profile is obtained directly from equation (14):

$$(\Delta\epsilon)_1 = \epsilon\left(\frac{\epsilon+2}{\epsilon+1}\right)\left(\frac{1}{2}\right)\left[3\csc^2\theta_1 + \Psi_1^2\tan^2\theta_1\right]\Phi^2 \tag{21}$$

2. <u>The Effect of a Finite Resolving Slit</u>

By considering a monoenergetic point source and an extremely narrow entrance aperture, the effect of the

finite width of the resolving slit is made to appear.

All the particles transmitted follow ultimate traces and the resolving slit passes them equally well. Since a finite number of particles are involved, the shape of this profile is therefore a rectangle.

Its width is also calculated from the equations of Section I. Those needed are:

$$x_1 = (Q_1 \cos\theta_1)\psi_1, \tag{3}$$

and

$$y_1 = (Q_1 \sin\theta_1)\sin\psi_1. \tag{4}$$

These are the equations that give the ultimate intersection of two traces coalescing to a single trace described by Q_1 and θ_1.

It is important to observe that the ratio of y_1 to x_1 is <u>independent of Q_1</u>. This means that after θ_1 has been selected all the ultimate intersections (for various Q's) lie on a cone with apex at the source. The semi-apex angle of the cone, α, is given by

$$\tan\alpha = y_1/x_1 = \tan\theta_1 \sin\psi_1/\psi_1. \tag{22}$$

Consider now a resolving slit that is also of infinitesimal width. Recalling that $Q = 2(p/Be)$ and that the amplitude of the ultimate trace is given by $R = Q_1 \sin\theta_1$, one can calculate the apparent change in energy (from a

monoenergetic source) corresponding to a displacement of the narrow resolving slit along the cone. One obtains:

$$\Delta x_1 = \psi_1 \cos\theta_1 \Delta Q_1 = \psi_1 \cos\theta_1 Q_1 \frac{\Delta p}{p}, \tag{23}$$

or

$$\Delta x_1 = \psi_1 \cos\theta_1 \frac{R}{\sin\theta_1} \left(\frac{\epsilon + 1}{\epsilon + 2}\right) \frac{\Delta \epsilon}{\epsilon}. \tag{24}$$

Hence the energy increment is given by

$$(\Delta \epsilon)_2 = \epsilon \left(\frac{\epsilon + 2}{\epsilon + 1}\right) \tan\theta_1 \frac{\Delta x_1}{\psi_1 R}. \tag{25}$$

This is also the energy width of the profile from a resolving slit of width Δx_1 and height Δy_1 disposed along the conical surface. Since such an aperture would be difficult to construct, the resolving slit used in the spectrometer opens in the axial direction. It is shown in Figure 20 along with the calculation relating its aperture to Δx_1.

3. The Effect of a Finite Source Size

Although the exact size of the source will be found intimately related with the magnitude of the entrance aperture and the width of the resolving slit, no rigid requirements are set on its shape by the permanent features of the spectrometer. Since the spectrometer has no preferred azimuth, it seems reasonable to assume axial symmetry for the source. It is also assumed small in relation to the

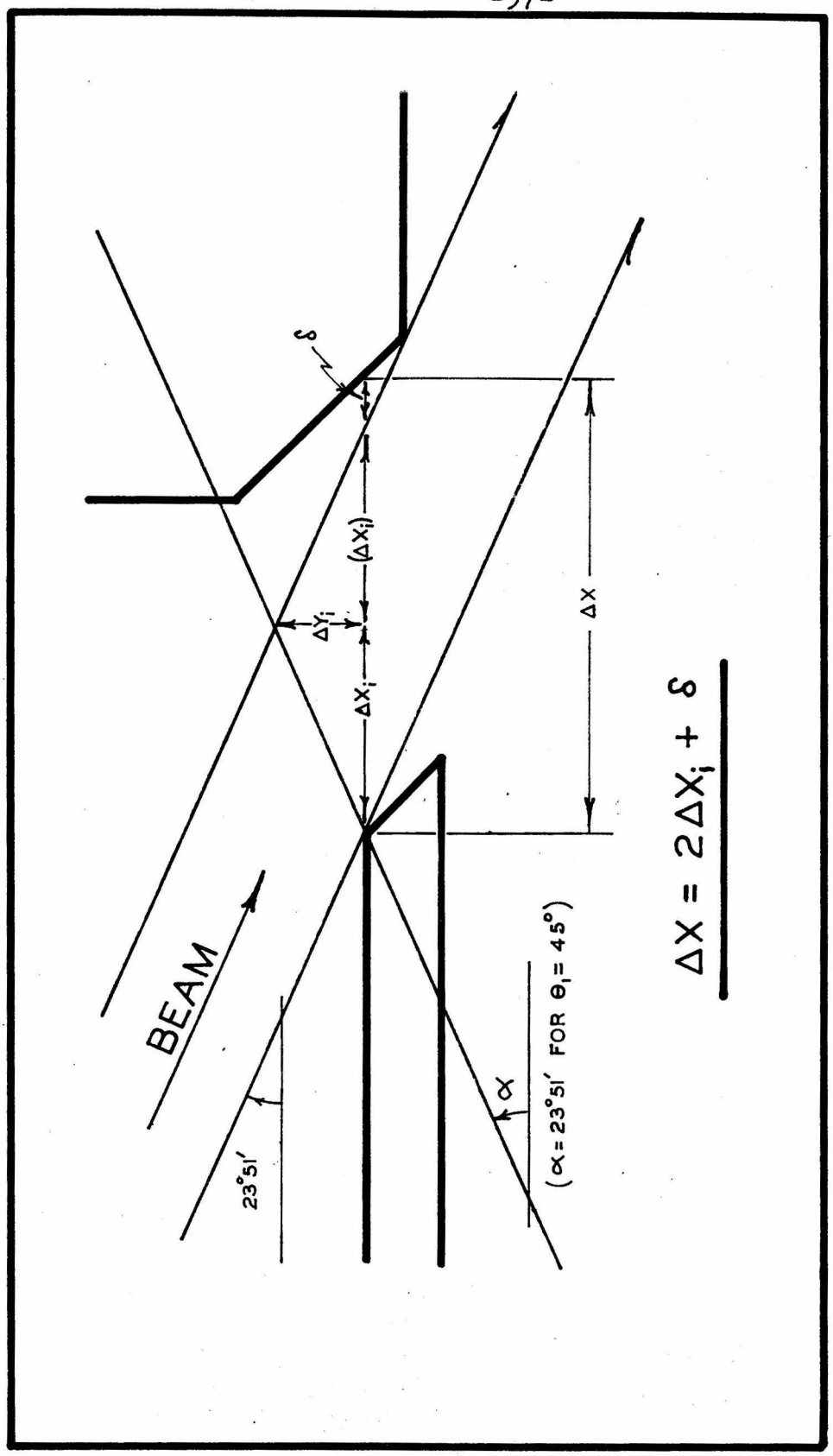

FIGURE 20. THE RESOLVING SLIT GEOMETRY.

dimensions of the instrument.

A shape of source consisting of a small, circular disk normal to the axis of the spectrometer was first proposed by Professor DuMond(1). Its effect is shown as follows.

Consider for the moment a monoenergetic point source and an infinitesimal solid angle and a similarly narrow resolving slit. Select the highest point of the resolving slit for consideration. The helical path of particles striking that point can be traced back to the source. A change in azimuth of $\psi_1 = 116^{\circ}14.3'$ will be traversed. Particles striking the top of the resolving slit leave the source at an angle of 45° with respect to the axis of the instrument. They also depart from the source at an azimuth $26^{\circ}14.3'$ below the horizontal.

Two views of this helical trajectory are shown in Figure 21 with a greatly enlarged disk source.

In this figure it is evident that a horizontal displacement of the entire trajectory displaces the point where it pierces the resolving slit along a line tangent to the slit.

On the other hand, a vertical displacement of the trajectory moves the point along a line normal to the slit. A displacement of the trajectory in this direction would no longer allow radiation of the same energy to pass through this element of the exit aperture.

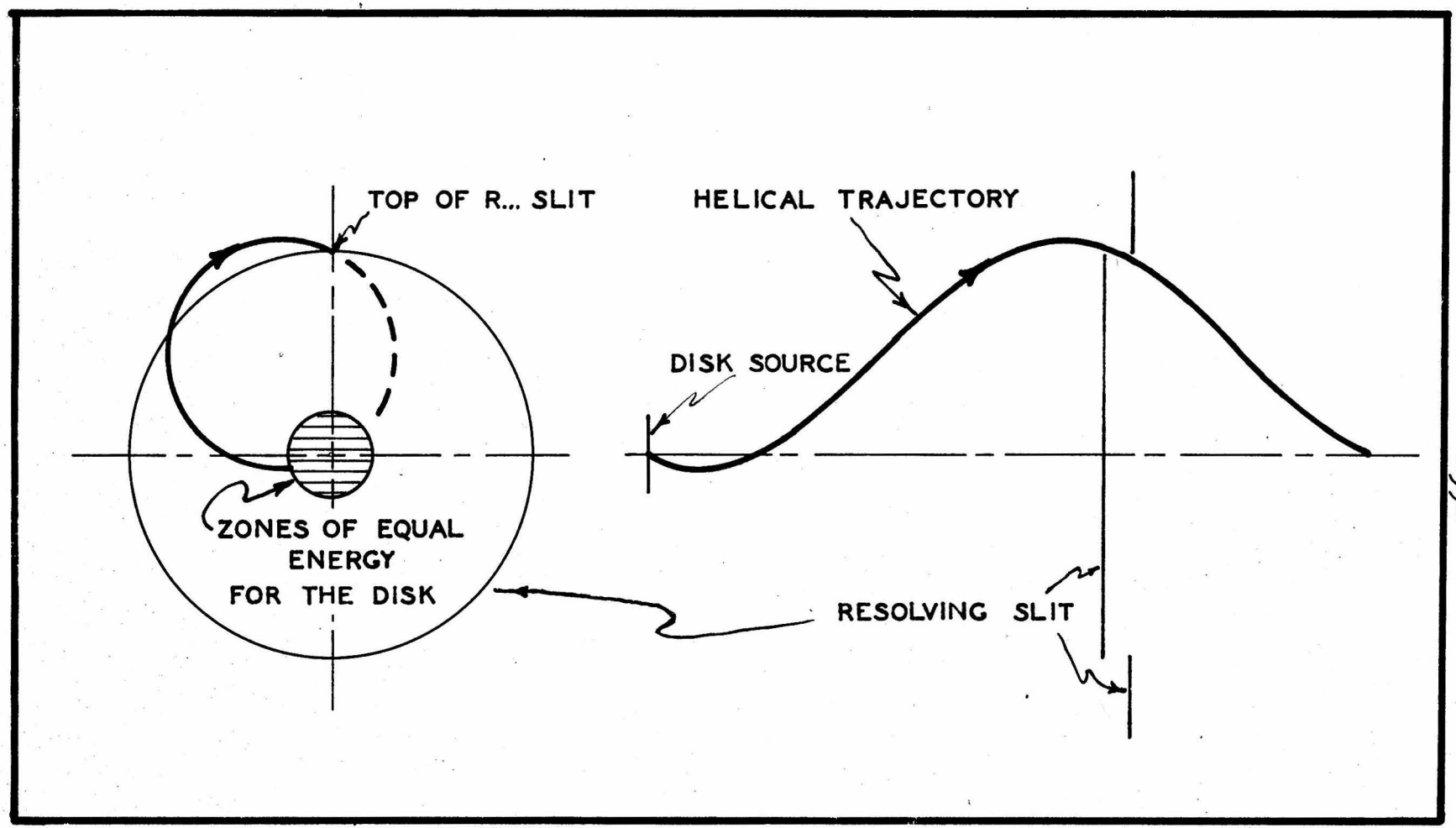

FIGURE 21. TWO VIEWS OF THE HELICAL TRAJECTORY.

Therefore, horizontal strips on the source are zones of the same energy for the topmost point of the resolving slit. Vertical displacements of the trajectory accordingly account for the line profile obtained for the source. Since there is no preferred azimuth for the spectrometer, all elements of the resolving slit are affected alike.

At first it might seem difficult to explore the source by translating the helical trajectory in a rigid manner. In fact, this is impossible with apertures of elemental width, for the translation of the helix would have to move the trajectory along the tangent to the edge of the entrance aperture for all displacements of the helix.

The dilemma is resolved by the following reasoning. Imagine the two extreme cases. In one, the exploration of the source moves the helix tangent to the edge of the entrance aperture and the exploration proceeds as if that aperture were not even present. At the other extreme, the trajectory is moved normal to the edge of the entrance aperture and is intercepted by it. However, another trajectory of only slightly different θ_1 (since the source is small) will be able to make its way through both of the apertures to the counter.

Since the resolving slit was placed at a focus making energy variations with θ_1 of second order, and since the

width of the source profile is a first order effect, this change in θ_1 is of no consequence. All other cases lie between these two extremes.

The semi-elliptical profile obtained by considering zones on the circular disk needs little comment. Its half width in terms of the source radius, ρ, is found from an equation developed in Section I,

$$y_i = (Q_1 \sin\theta_1) \sin\psi_i. \tag{4}$$

The first order effect of the finite area of the source is to change the effective radius of the resolving slit for particles leaving its edge. Hence,

$$\Delta y_1 = (1+\cot^3\theta_1)^{-1}\rho \; {}^{*} = \sin\theta_1 \sin\psi_i \Delta Q_1$$

$$= \sin\theta_1 \sin\psi_i Q_1 \frac{\Delta p}{p} = \sin\theta_1 \sin\psi_i \frac{R}{\sin\theta_1}\left(\frac{\epsilon+1}{\epsilon+2}\right)\frac{\Delta\epsilon}{\epsilon}$$

Then the source profile <u>half-width</u> (since the source radius is used) is given by:

$$(\Delta\epsilon)_3 = \epsilon\left(\frac{\epsilon+2}{\epsilon+1}\right)\frac{\rho}{(1+\cot^3\theta_1)R\sin\psi_i} \tag{26}$$

$R\sin\psi_i$ is equal to the radius of the resolving slit. $(\Delta\epsilon)_3/\epsilon$ is usually about one percent. This justifies

---

*Δy_1 infers displacement of the resolving slit along the cone of semi-apex angle K. This is shown in Figure 20.

the earlier treatment that assumed the source size to be small.

These three individual profiles are shown as Figure 22.

B. The Instrumental Profile Using a Disk Source

Each of the three profiles of Figure 22 was obtained by a construction independent of the coordinates on which the other two depend. Hence when all are present simultaneously the resultant profile is given by the fold of the three individual profiles. Professor DuMond has calculated this instrumental profile[1], and it is given as Figure 23.

Figure 23 also shows the profile obtained by folding just the entrance aperture and the resolving slit into each other. It was shown that the fold of these two has maximum height with narrowest half-maximum width when $(\Delta\epsilon)_1 = (\Delta\epsilon)_2$.

Then when the fold of these two is in turn folded with the elliptical source profile, Professor DuMond showed that the resultant instrumental profile would yield the greatest counting rate with least half-maximum width when $(\Delta\epsilon)_1 = (\Delta\epsilon)_2 = (\Delta\epsilon)_3$. The pair first folded, the source profile, and the resultant fold of the three are all shown in Figure 23.

For these widths, the half-maximum width of the instrumental profile is $(\Delta\epsilon)_I = 1.62(\Delta\epsilon)_1$.

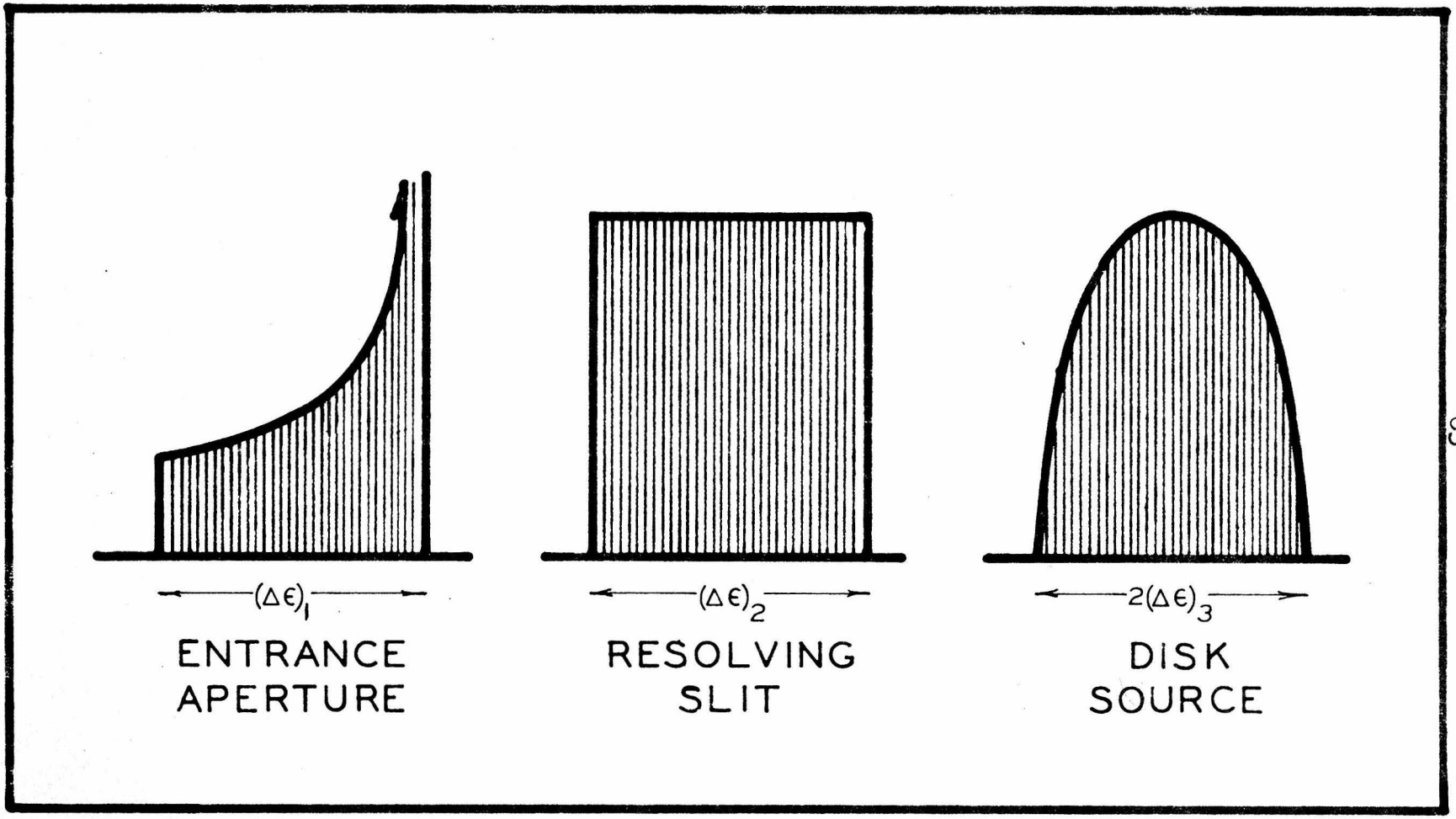

FIGURE 22. THE THREE INSTRUMENTAL CONTRIBUTIONS TO THE LINE PROFILE.

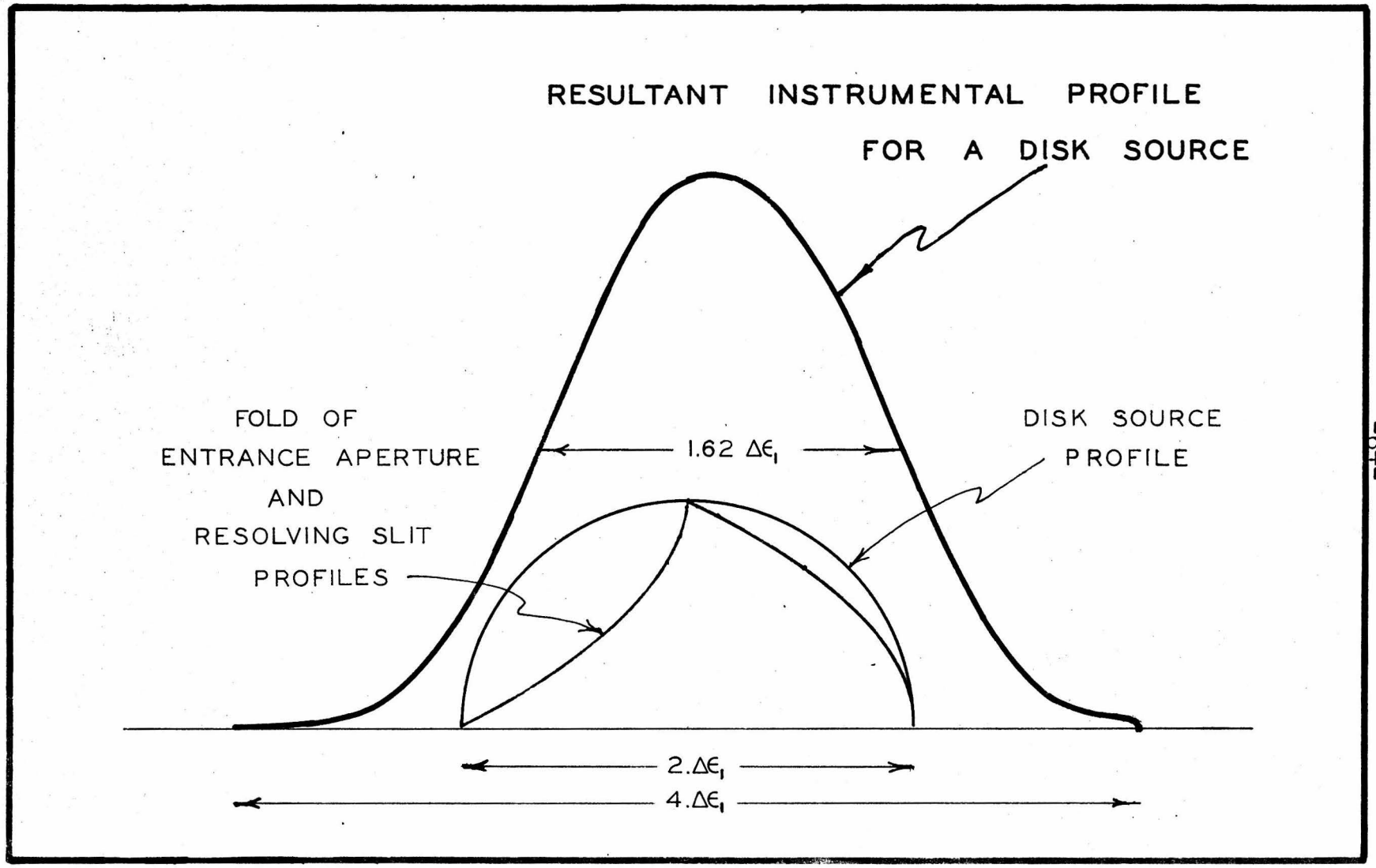

FIGURE 23. THE INSTRUMENTAL PROFILE FOR A DISK SOURCE.

C. The Conical Source and Its Profile

An entirely new shape of source was suggested by Dr. D. E. Muller not long before the initial operation of the spectrometer was begun.

Dr. Muller's proposal was that the radioactive material of the source should be distributed on the surface of a cone having a semi-apex angle with tangent equal to the slope of the ultimate trace at the resolving slit. This is illustrated in Figure 24.* With a monoenergetic source of this type, the last elements of the source contributing ultimate traces passing over the inner defining edge of the resolving slit (as the magnetic field is increased) lie along a strip of finite length on the cone. Furthermore, since these last elements leave the cone tangent to its surface, the zones on the cone appear to have an infinite specific activity.

The profile of the cone source is shown as Figure 25. Its similarity to the entrance aperture profile is even greater than the figure shows, for both of these profiles have the same inverse square root dependence on energy near their singularities.

---

*Figure 24 is somewhat misleading in that it fails to show the helical trajectories and the fact that the particles of interest leave the cone surface nearly tangent to it.

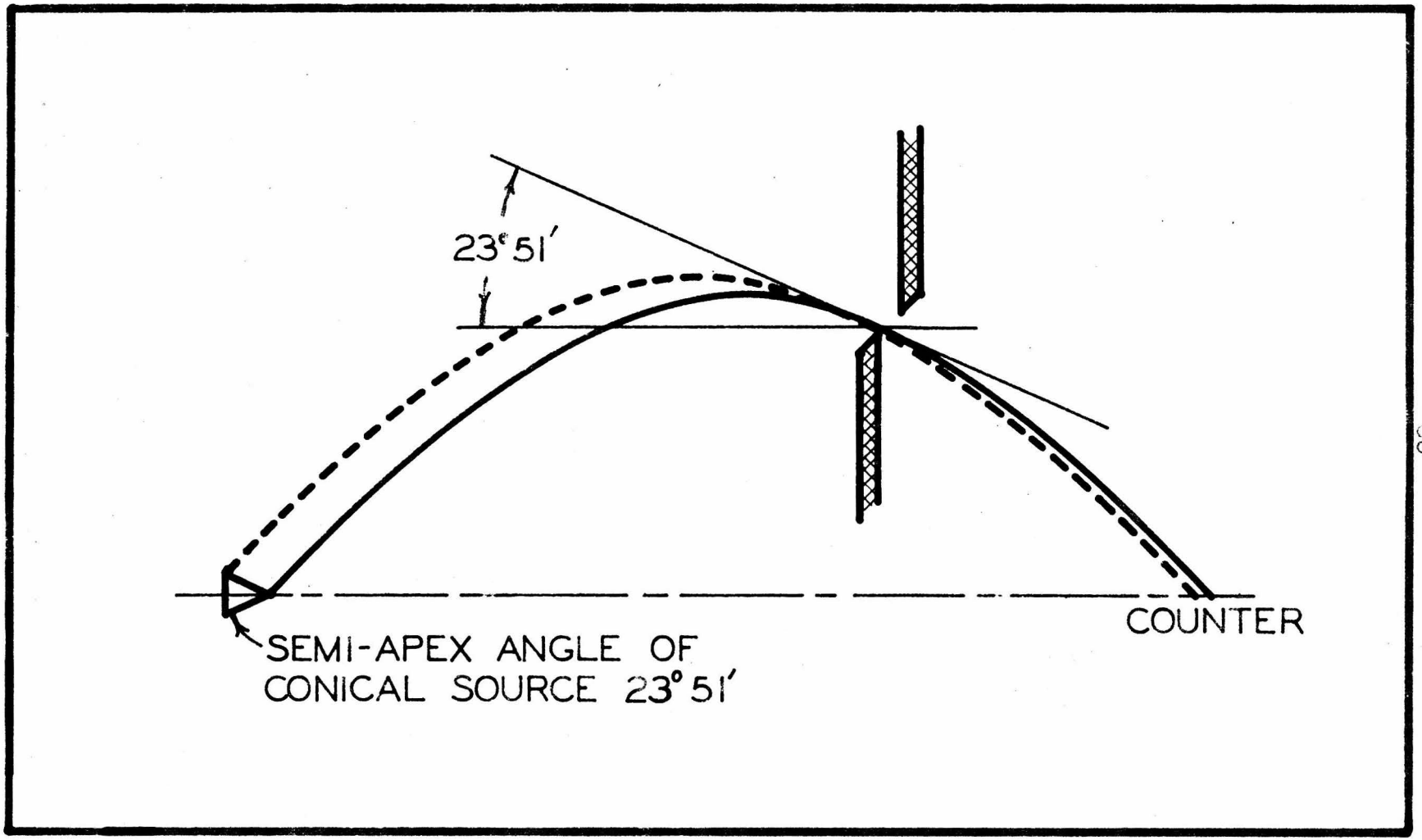

FIGURE 24. AN ILLUSTRATION OF THE SEMI-APEX ANGLE CHOSEN FOR THE CONE SOURCE.

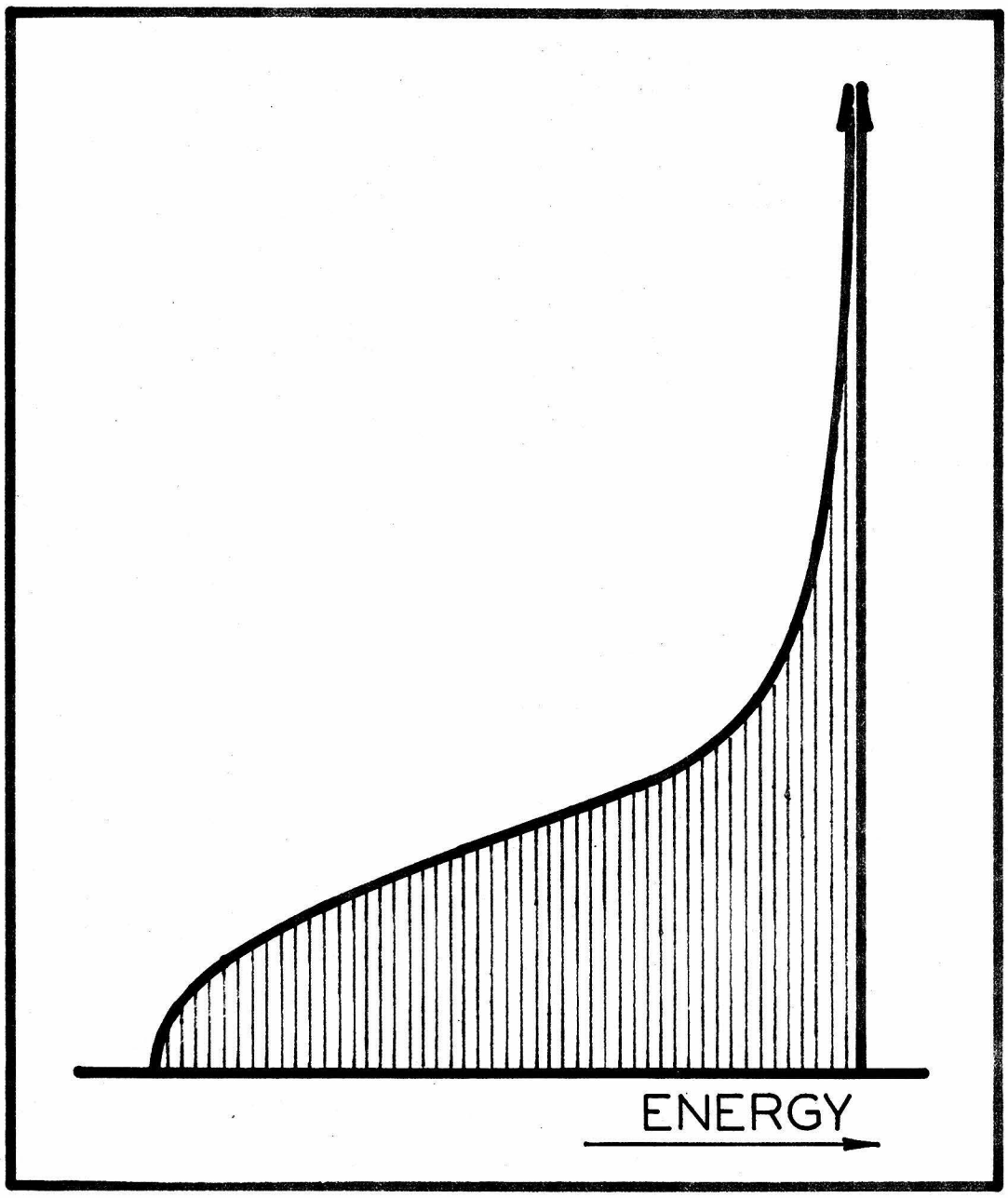

FIGURE 25. THE PROFILE FOR A MULLER-TYPE CONE SOURCE.

This source profile has a curious and a very fortunate effect. When folded with the entrance aperture, the resultant profile is rectangular on the high energy side for nearly half of its width.*

When folded with that of the resolving slit, which is also rectangular, the instrumental profile is found to have a very straight leading edge of finite slope. This profile is shown in Figure 26.

The profile of Figure 26 would be observed only if a perfectly monoenergetic source were used. Of course, such sources are impossible to construct. Fortunately, however, a source very nearly realizing this characteristic has been obtained. With it, profiles having the long straight leading edge of Figure 26 have been observed experimentally. The construction of this source is described in the next section.

The straight leading edge can be interpreted in a very useful way. Its intersection with the horizontal axis on the high energy side corresponds to the situation where the discontinuities of the two inverse square root profiles just begin to overlap an edge of the resolving slit profile.

---

*These two are folded so that the high energy side of the resultant occurs when only the two singularities overlap. This is interpreted to mean that the very last elements of the cone (assuming increasing field) are transmitted along ultimate traces.

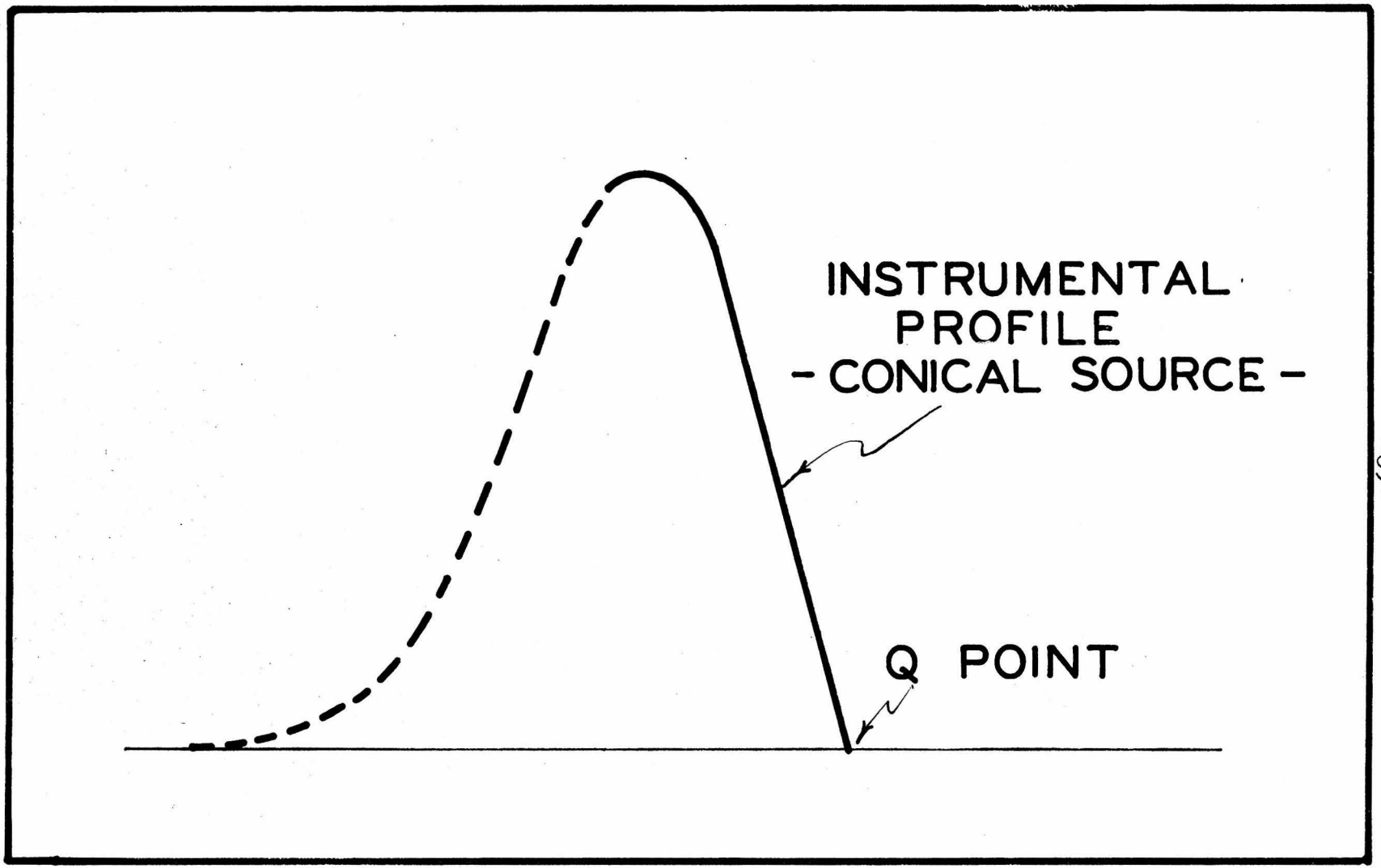

FIGURE 26. THE INSTRUMENTAL PROFILE FOR A CONE SOURCE

This is precisely the condition one desires to measure since then only particles from the tip of the source (and a line element extending along the source from the tip) pass exactly along ultimate traces that just clear the inner defining edge of the resolving slit.

Hence the characteristic fiducial point is obtained by constructing the intersection of the straight leading edge of the observed profile with the horizontal axis.* This intersection point has been named the Q-point.

*In practice, the background level or beta-ray continuum superimposed on the line is assumed to have constant slope over distances equal to the line width.

V. PRELIMINARY MEASUREMENTS OF THE F AND I LINES OF THORIUM

The first observations with the new spectrometer were made with a Muller-type cone source that was turned from aluminum alloy stock. It was activated by electro-depositing ionized Thorium-A on it from Thoron gas.

Since a very thin surface layer of the radioactive substance was deposited, the calculated instrumental profile was broadened little by energy loss in the source. In fact, the observed profile shown in Figure 27 is very like the calculated instrumental profile. Its straight leading edge clearly is sufficiently long for the construction that is used to determine the fiducial Q-point.

The added feature of the observed profile is a fillet shown at the intersection of the straight line portions. Several explanations have been given for its appearance. The fillet might be ascribed to irregularities in the resolving slit or to de-centering of the source. However, profiles obtained by measuring radiation in selected azimuthal sectors of the beam show that this effect is not large. The maximum variation in the relative radial position of the source and resolving slit has been found to be less than half a thousandth of an inch after centering. The fillet might also be attributed in part to slight

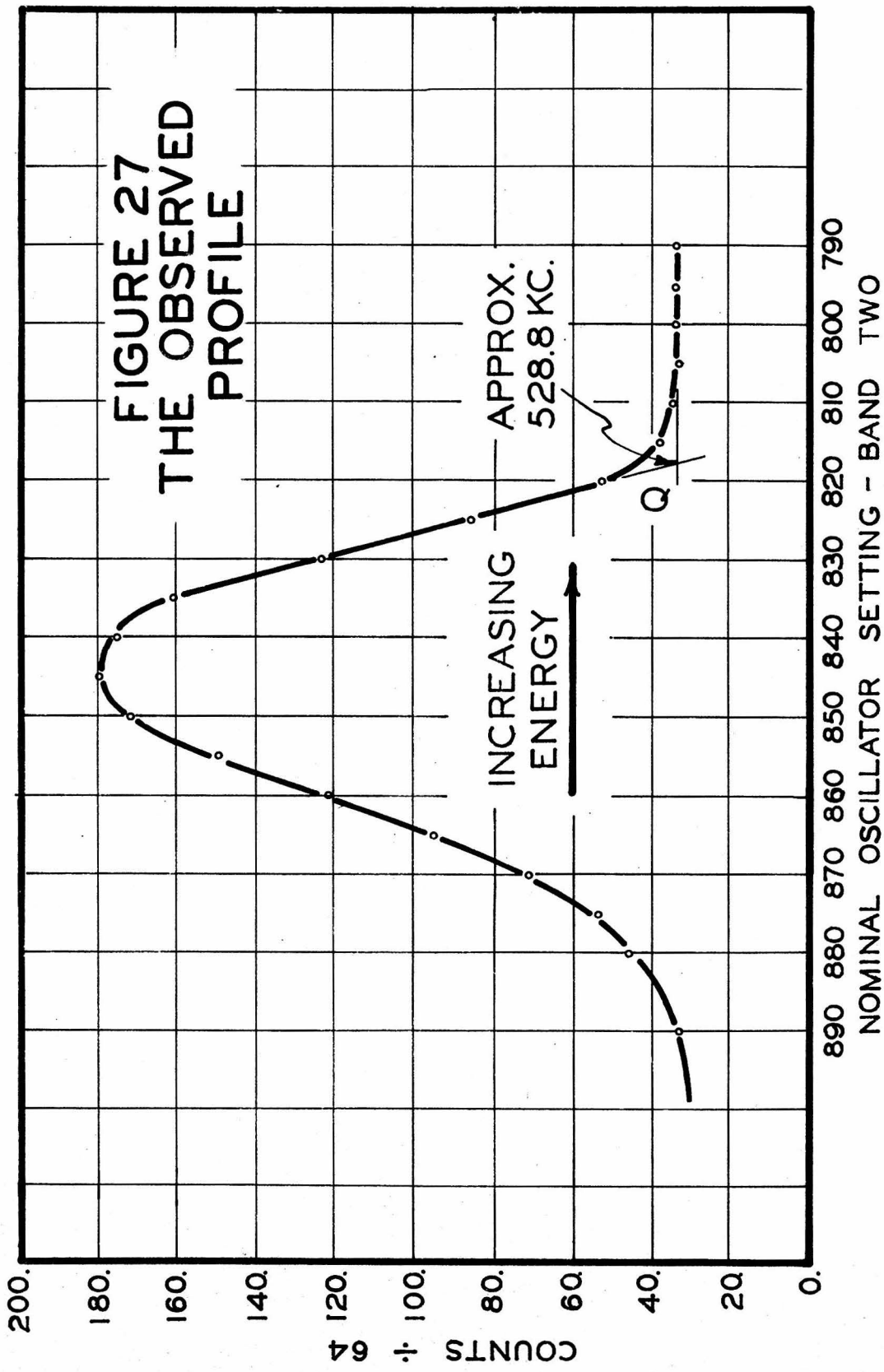
FIGURE 27
THE OBSERVED
PROFILE
APPROX.
528.8 KC.
Q
INCREASING
ENERGY
COUNTS ÷ 64
200.
180.
160.
140.
120.
100.
80.
60.
40.
20.
0.
890 880 870 860 850 840 830 820 810 800 790
NOMINAL OSCILLATOR SETTING - BAND TWO

fluctuations in the magnetic field, a result of noise superimposed on the proton resonance signals. It has also been suggested that a possible explanation for a portion of it may lie in the finite width of the electronic levels of the atom, since the excited atomic states have a finite lifetime after the conversion electrons are ejected. Probably a combination of these effects explains the fillet.

A. Two Search Runs With the Thorium Source

1. A Search With Coarse Resolution

The lower energy portions of a coarse search run with the Thoron-deposited source are shown as Figure 28. Observations extend to about 500 Kev at the right edge of the figure. The very strong F and I lines* are evident above the other lines in the figure. They are used for the measurements reported in the following paragraphs of this section.

If extended to lower energies, Figure 28 would show that the softest beta-rays of the continuous spectrum begin to make their way through the wall of the counter at about 50 Kev. A K-to-L conversion ratio of roughly seven has been reported for the F and I lines.(15) Hence it is evident from the figure that a significant portion of the

---

*(Ellis notation). The F and I lines are K and L conversion lines of a nominal 238 Kev gamma-ray of Thorium-C.

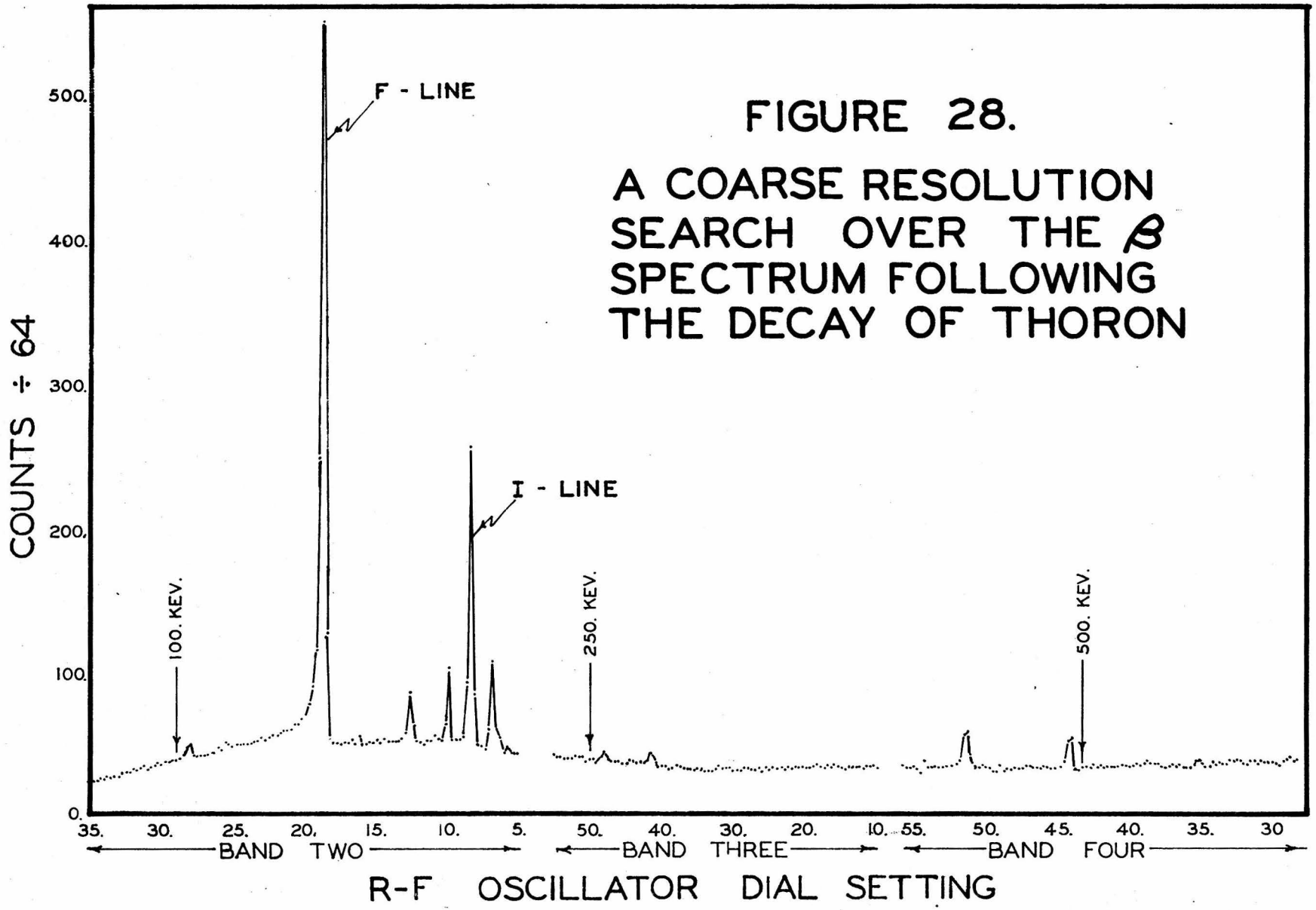

FIGURE 28.

A COARSE RESOLUTION SEARCH OVER THE β SPECTRUM FOLLOWING THE DECAY OF THORON

F line is intercepted by the window of the counter.

The observations of Figure 28 were made with an aluminum cone source of one-eight inch base diameter. Its activity was estimated as roughly 0.25 millicuries. The spectrometer aperture was set to accept radiation from 2.5 percent of the total sphere about the source. Other instrumental settings were adjusted in proportion. Counts were recorded for a 32-second interval for each point shown. Between adjacent points the proton resonance frequency was shifted by an increment varying from one-fourth to one-half a percent of the resonance frequency. The abscissae, given as oscillator dial divisions, are roughly proportional to the r-f frequency.

2. A Search With Fine Resolution

A 233 Kev gamma-ray reported as the E_d line of Thorium is believed to occur in stable Pb^{208} following beta-decay from Thorium-C"(15). If resolved, its K-conversion line should be observed on the low energy side of the strong F-line.

Figure 29 shows the result of a search over this portion of the spectrum. The frequency width of the F-line was observed as 0.35%. A conical source of 1.0 mm base diameter was used with other instrumental parameters set accordingly. Counts were recorded during two-minute inter-

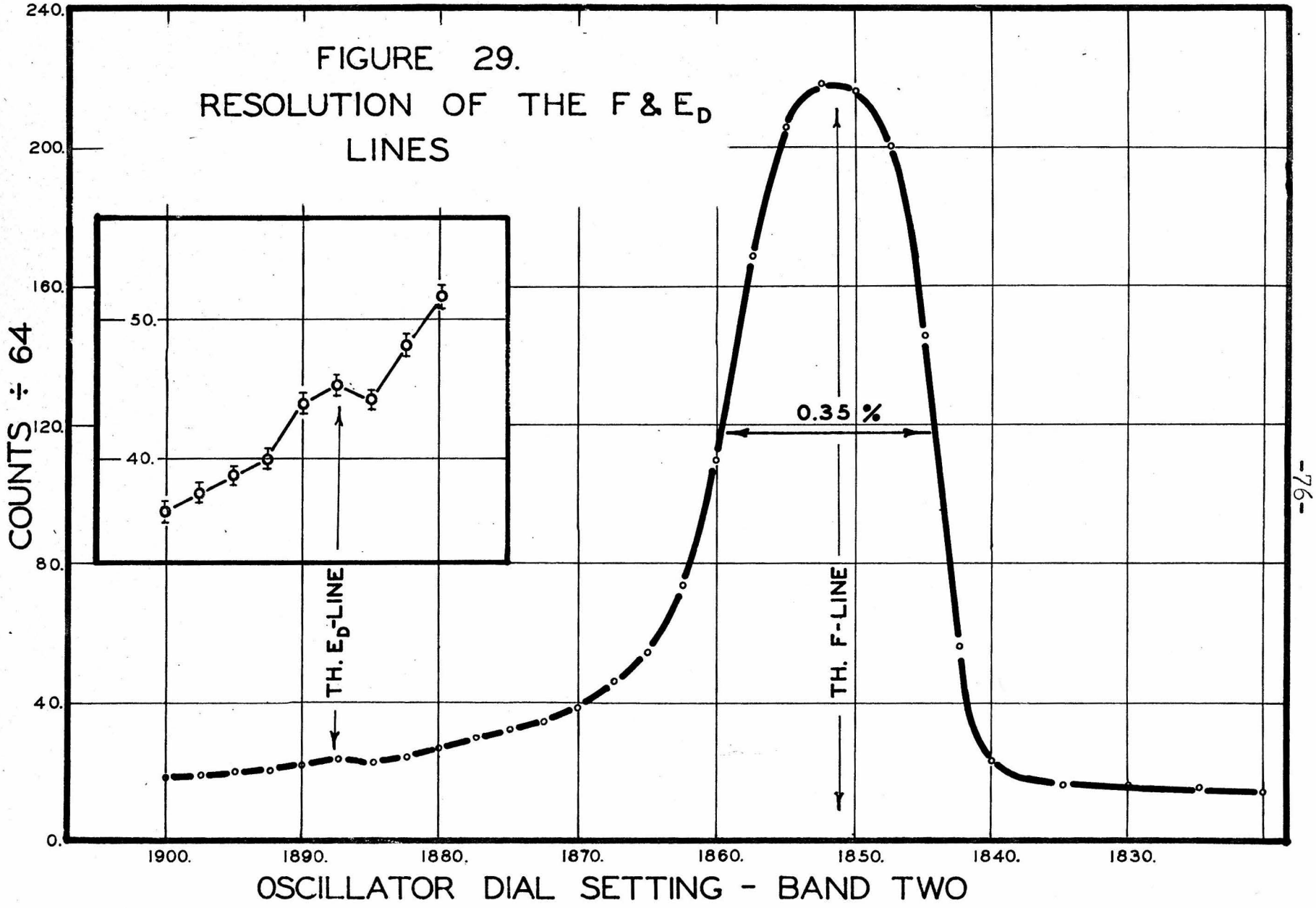
FIGURE 29.
RESOLUTION OF THE F & E_D LINES
COUNTS ÷ 64
240.
200.
160.
120.
80.
40.
0.
50.
40.
0.35 %
TH. E_D-LINE
TH. F-LINE
1900.
1890.
1880.
1870.
1860.
1850.
1840.
1830.
OSCILLATOR DIAL SETTING - BAND TWO

vals at each setting along the F-line. Over the E_d line, four-minute counting intervals were used for each observation. The data for the observations near the E_d line are correctly shown in the insert of Figure 29. The results for the four-minute intervals were halved and plotted as a continuation of the F-line to show the relative intensities of the two lines.

B. The Reproducibility of Repeated Observations of the Thorium F and I Lines

The profiles of the F and I lines were observed on four successive days. Six profiles were obtained for each of the two lines.

The source was removed from the spectrometer and a newly activated one was re-inserted for each day's observation. Between runs made on the same day, the source insertion-rod was retracted and again re-seated against the tapered conical socket in the source assembly. This subjected the whole procedure of source installation to the test of reproducibility.

The quality of the data obtained is shown in Figure 30, which shows the leading edge of the I-line as observed during a typical run.

The twelve Q-points were determined graphically. Their construction gave the Q-point frequencies to five

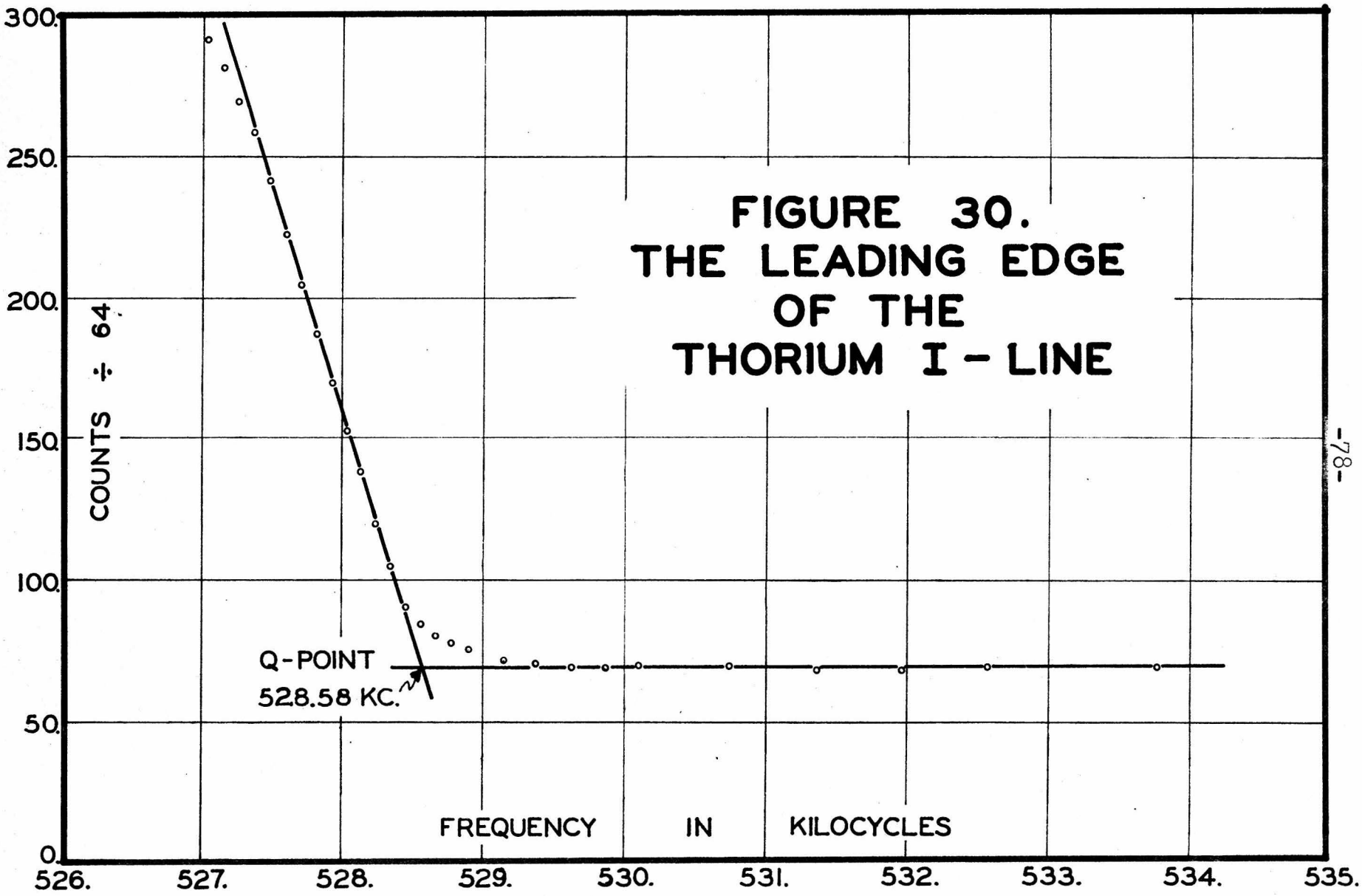

FIGURE 30.
THE LEADING EDGE
OF THE
THORIUM I - LINE

significant figures with considerable certainty. This data is given in Table I. The table also gives the mean Q-point, the calculated standard deviation of a single observation, and the standard deviation of the mean for both the F and I lines. A normal distribution and the absence of systematic errors were assumed in computing the errors.

The $(H\rho)$ ratio for the F and I lines is calculated from the data of Table I and compared with two other recent determinations in Table II.

The agreement is reasonably satisfactory. However, the error of the value computed from Table I assumes that no systematic errors were present. This may well be an invalid assumption. Frequencies were measured with a war-surplus, U. S. Army Signal Corps, Model BC-221-T frequency meter. To measure frequencies with this meter, one is required to adjust the frequency of its variable-frequency oscillator to coincidence with that of its standardizing crystal oscillator at a "check point" near the frequency that is to be measured. Adjacent calibration points on each side of the unknown frequency were found to disagree as much as several hundred cycles for the frequencies of interest. The BC-221-T provides no adjustment for correcting this defect. Hence, an "average" alignment was attempted. This procedure could easily be responsible for a systematic error of several parts in 10^5.

TABLE I

REPRODUCIBILITY OF MEASUREMENTS OF THE F AND I LINES

Run No.	Date	F-Line Q-Point	I-Line Q-Point
1	27 March	418.42 kc.	528.65 kc.
2	28 March	418.42 kc.	528.59 kc.
3	31 March AM	418.48 kc.	528.67 kc.
4	31 March PM	418.38 kc.	528.60 kc.
5	1 April AM	418.43 kc.	528.58 kc.
6	1 April PM	418.40 kc.	528.58 kc.

Line	Mean Q-Point	S.D.(Single Obs.)	S.D.(Mean)
F	418.422 kc.	± 0.034 kc.	± 0.014 kc.
I	528.612 kc.	± 0.039 kc.	± 0.016 kc.

TABLE II

THE RATIO OF $(H\rho)$'S FOR THE F AND I LINES

$(H\rho)I/(H\rho)F$	Probable Error	Measured By:
1.26319	± .00005	G. Lindstrom (16)
1.26317	± .00012	H. Craig (17)
1.26335	± .00004	Table I.

A Hewlett-Packard, Model 524A, Frequency Counter now on order will soon eliminate the possibility of an error from this source.

C. The Calculated Difference in the K and L_I Binding Energies for Thorium-C (Bismuth^{212}).

The possibility of a small systematic error in the Q-point frequencies of Table I casts some doubt on the reliability of further calculations made with them. However, this error must be very small, and the validity of the binding energy calculation suffers from far more serious objections. These objections will be discussed as they appear in the calculation. It is believed that worthwhile inferences may be made with answers obtained in this way.

Assuming a perfectly homogeneous magnetic field, the kinetic energies of the particles of the F and I lines can be calculated from their Q-point frequencies by using the relation

$$E_{kin} = m_o c^2 \left(\sqrt{1 + \left(\frac{pc}{m_o c^2} \right)^2} - 1 \right)$$

$$= m_o c^2 \left(\sqrt{1 + 2 \left(\frac{\rho e}{m_o c^2} \frac{2\pi f}{\delta p} \right)^2} - 1 \right), \qquad (27)$$

This equation applies to a "45°" spectrometer with proton-moment measured magnetic field.

The difference in the K and L_I binding energies is then given by

$$E_{kl} = m_o c^2 \left(\sqrt{1 + 2\left(\frac{\rho e}{m_o c^2} \frac{2\pi f_I}{\gamma_f}\right)^2} - \sqrt{1 + 2\left(\frac{\rho e}{m_o c^2} \frac{2\pi f_F}{\gamma_p}\right)^2} \right). \qquad (28)$$

The error of equation (28) is dominated by the errors of f_I, f_F, and ρ. The probable errors for the two frequencies are obtained from the data of Table I.* A probable error is assigned to ρ as follows. The measured diameter of the inner edge of the resolving slit is 14.089 inches. This is nearly twice the amplitude of the trace and four times ρ. It is assumed that the dimension given by the measurement is within 0.001 inches of the true value. This is not unreasonable. A probable error one-fourth as large is then assigned to ρ. Hence ρ equals (9.9743 ± .0006$\frac{4}{}$) centimeters.

Assuming that the errors are independent, the error of E_{kl} is $\sigma_{E_{kl}}$, where

$$\sigma_{E_{kl}}^2 = \sum_i \left(\frac{\partial E_{kl}}{\partial q_i}\right)^2 \sigma_{q_i}^2 . \qquad (29)$$

The q_i are the error-contributing quantities, f_F, f_I, and ρ.

*The Standard deviation of the mean is multiplied by 0.6745 to get the probable error for each frequency.

The value of the energy obtained from equations (28) and (29) is given in Table III with three other recent determinations of the K and L_I binding energy difference. The error calculated for E_{kl} is small indeed.

TABLE III

THE K AND L_I BINDING ENERGY DIFFERENCE FOR BISMUTH

Energy Difference	Measured By:
74.490 Kev	Y. Cauchois et H. Hulubei *(18)
74.154 Kev	R. D. Hill et all **(19)
74.128*.010 Kev	Y. Cauchois ***(17)
73.990*.013 Kev	The data of Table I and ρ.

Little agreement is evident in Table III. Although the results obtained from X-ray work seem to be converging on a value, its magnitude does not seem to be confidently known as yet. This is not unreasonable, for the precise measurement of absorption edges is difficult, and the results depend upon interpretation somewhat.

Several observations can be made concerning the energy difference computed from the Q-point frequencies. The disagreement of Table III can scarcely be due to an uncer-

*The DuMond and Cohen(20) latest (May 1951) values for λ_g/λ_s and λ_o were used in converting this data.
**Hill and co-workers(19) used the DuMond and Cohen(20) values for converting Seigbahn's data(21).
***Private communication to H. Craig(17).

tainty in the frequencies, i.e., to a possible systematic error, for this assumption makes matters worse. If Table II were used to infer a correction in the Q-point frequencies, the F and I lines would have energies more nearly equal, and the inferred binding energy difference would be even less.

Furthermore, the resolving slit diameter is certainly not in error by an amount sufficient to explain the discrepancy. One might argue that a ρ determined from the slit diameter is in error for other reasons.

If the axial position of the source were in error, a different ρ would then occur. However, it is believed that the axial position of the source is known within a few thousandths of an inch by direct micrometer caliper measurements of the machined parts of the spectrometer. The accumulated error in these measurements should be no greater than a few thousandths of an inch. An error much larger than this is required to explain the discrepancy.

An error in ρ due to an inhomogeneity of the field does not seem to resolve the problem either. This reasoning is as follows. The proton samples are located very near the center of the spectrometer. It would seem reasonable to assume that an inhomogeneous field would be stronger in these central regions than at the beta-particle trajectories. (The coil disposition shown in Figure 4 might be

used for such a qualitative argument.) This would mean weaker fields at the trajectories (than the fields measured by the proton samples). This would mean helices of larger ρ. Hence higher Q-point frequencies would be observed with the inhomogeneous field.

This would mean that the actual F and I line kinetic energies would be less than those inferred from the frequencies of Table I assuming a homogeneous field. This whole line of reasoning presents a new dilemma. The sum of the F-line kinetic energy (computed from the frequencies of Table I and equation (28)) and the largest K absorption-edge energy given by any of the authors of Table III is at present over 350 volts less than the precisely known energy of the gamma-ray.* Hence this explanation does not seem to resolve the dilemma.

Still another factor may be involved. It would seem necessary to advance some argument for assuming that the exact energies given by absorption-edge measurements are valid for this calculation. The Thorium-C atom that ejects the internal conversion electron is created by beta-decay. It would seem that the K and L_I energy levels at the time of conversion might not be those implied by the use of

---

This is given as 238.595~.060 Kev by Klein(22) after revision due to recent calibration of the curved-crystal spectrometer(23). Dr. Klein has not yet assigned the error.

absorption edges if sufficient time does not elapse between the beta-ray and internal conversion processes.

The problems of the preceding paragraphs will not be followed further at this time. There are still too many uncertainties involved (due to the newness of the instrument), and further discussion would be even more speculative.

It is important to realize that the precision of future measurements does not depend on the homogeneity of the spectrometer field. Numerous sources emitting gamma-radiation of precisely known wavelength have been measured with the curved-crystal spectrometer. With the beta-ray spectrometer, the ratio between the momentum of the calibrating particles and that of other particles being studied will be given simply as the ratio of two precisely measured frequencies. This does not assume either a homogeneous field or a magnitude for ρ.

On the other hand, if further tests show that the field can be considered perfectly homogeneous by assigning an "effective ρ" to the instrument (to take account of a slight inhomogeneity in the field), an alternative method using an equation similar to (28) might prove advantageous. If one would use the same element as an external converter for both sources, it would seem that the calculation of the energy would not involve an exact knowledge of the

absorption edge involved, for the same energy would be required to extract the conversion electrons from the material of both sources. This would appear to remove some of the difficulties found earlier.

In any event, however, it is believed that the homogeneous magnetic field beta-ray spectrometer will prove a most useful and precise companion for the curved-crystal instrument.

APPENDIX I

COILS FOR REMOVING THE RADIAL COMPONENTS OF THE EARTH'S MAGNETIC FIELD FROM THE SPECTROMETER.

If the length of the side of the flat, square coil of Figure 31(a) is given by $\underline{a}$, and $\underline{x}$ is the distance from its center along its axis, the magnetic induction along the axis is given by:

$$B(x) = \frac{2\mu I}{\pi\sqrt{\frac{a^2}{2}+x^2}} \cdot \frac{\left(\frac{a}{2}\right)^2}{\left(\frac{a}{2}\right)^2+x^2} \qquad (30)$$

This is found by superimposing the effects of the four straight sides of length $\underline{a}$.

Equation (30) has two points of inflection at $x = \pm x_1$, where

$$\frac{x_1}{(a/2)} = 0.5445 = \alpha \qquad (31)$$

Hence by placing two square coils on the same axis in planes parallel to each other at a distance $2x_1 = 0.5445a$ apart, one obtains a uniform field at their center. The magnitude of the field at the center is given by:

$$B_{center} = \frac{8I}{\pi a\sqrt{2+\alpha^2}\,(1+\alpha^2)} = \frac{2I}{\pi a}(2.0359) \qquad (32)$$

where rationalized mks units are used. This arrangement

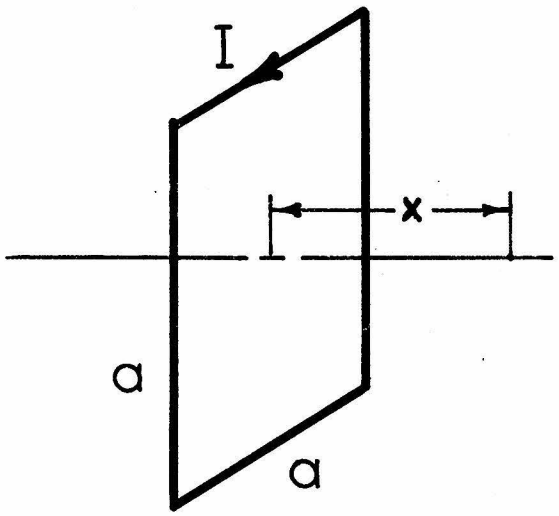

Fig. 31(a)

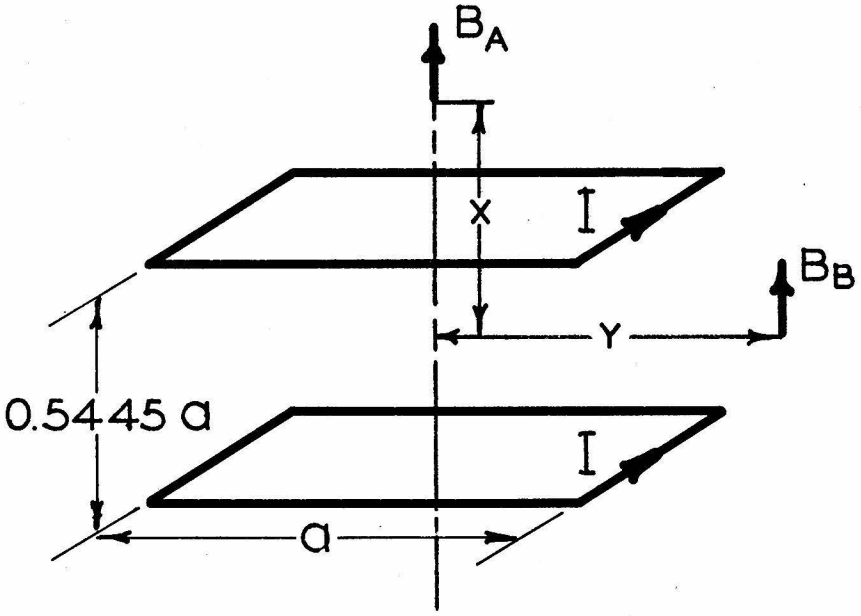

X = DISTANCE FROM CENTER ALONG AXIS

Y = DISTANCE FROM CENTER PARALLEL TO COIL SIDE IN CENTRAL PLANE

Fig. 31(b)

FIGURE 31. THE GEOMETRY AND NOMENCLATURE OF THE SQUARE COIL PAIRS.

is shown in Figure 31.

The currents in these coils are adjusted by means of a null-indicating wind-driven generator that is mounted 12.5 inches away from the center of the coils, below the spectrometer. Hence it is necessary to know the magnitude of the field of the coils at points other than their center in order to determine the corrections to the indicated null value of current.

For the displacements $\underline{x}$ and $\underline{y}$ shown in Figure 31 the same superposition process yields the relations:

$$B_A = \frac{2I}{\pi a}\left[\frac{2}{\sqrt{2+\left(\frac{2x}{a}-\kappa\right)^2\left(1+\left[\frac{2x}{a}-\kappa\right]^2\right)}}\right. \tag{33}$$

$$\left. + \frac{2}{\sqrt{2+\left(\frac{2x}{a}+\kappa\right)^2\left(1+\left[\frac{2x}{a}+\kappa\right]^2\right)}}\right]$$

$$B_B = \frac{2I}{\pi a}\left[\frac{\left(1+\frac{2y}{a}\right)}{\sqrt{\left(1+\frac{2y}{a}\right)^2+1+\kappa^2}}\left(\frac{1}{\left(1+\frac{2y}{a}\right)^2+\kappa^2}+\frac{1}{1+\kappa^2}\right)\right. \tag{34}$$

$$\left. + \frac{\left(1-\frac{2y}{a}\right)}{\sqrt{\left(1-\frac{2y}{a}\right)^2+1+\kappa^2}}\left(\frac{1}{\left(1-\frac{2y}{a}\right)^2+\kappa^2}+\frac{1}{1+\kappa^2}\right)\right]$$

These formulae are checked by the fact that they reduce to the form given for B_{center} at $x = y = 0$.

The current corrections computed from (33) and (34) become a part in 10,000 of the main spectrometer field at spectrometer fields of about 8 gauss. Since magnetic fields of less than 35 gauss are never used, the corrections have never been necessary. However, the result of the calculation of the corrections does serve to assure one of the homogeneity of the field of the square coils within the spectrometer.

APPENDIX II

THE DOUBLE-HELMHOLZ SWEEP COILS

Professor Davis' original calculation for the field of these coils can be outlined as follows.

Professor W. R. Smythe's text[24] gives an expansion for the vector potential of a circular loop of current I in spherical harmonics. It is

$$r<a \quad \underset{\sim}{A} = \underset{\sim}{\phi} \frac{\mu I}{2} \sum_{n=1}^{\infty} \frac{\sin\alpha}{n(n+1)} \left(\frac{r}{a}\right)^n P_n^1(\cos\alpha) P_n^1(\cos\theta). \qquad (35)$$

in mks units. The quantites $\underline{a}$ and $\underline{\alpha}$ are the radius vector and co-latitude angle of the loop. $\underline{r}$ and $\underline{\theta}$ are the spherical polar coordinates.

The geometry and nomenclature of the double-Helmholz sweep coils are given in Figure 32.

The terms for even n vanish for the symmetrical arrangement of Figure 32, for $P_n^1(\cos\alpha)$ is an odd function about $\pi/2$ when n is an even integer.

Hence, one can obtain the following expressions for the radial component of the magnetic induction of the set of four coils shown in Figure 32:

$$r<a \quad B_r = \mu(\sin\alpha) \sum_{n\,odd}^{\infty} \left[\frac{I_1}{a}\left(\frac{r}{a}\right)^{n-1} - \frac{I_2}{b}\left(\frac{r}{b}\right)^{n-1}\right] P_n^1(\cos\alpha) P_n(\cos\theta) \qquad (36)$$

$$r>b \quad B_r = \mu(\sin\alpha) \sum_{n\,odd}^{\infty} \left[\frac{I_1}{a}\left(\frac{a}{r}\right)^{n+2} - \frac{I_2}{b}\left(\frac{b}{r}\right)^{n+2}\right] P_n^1(\cos\alpha) P_n(\cos\theta) \qquad (37)$$

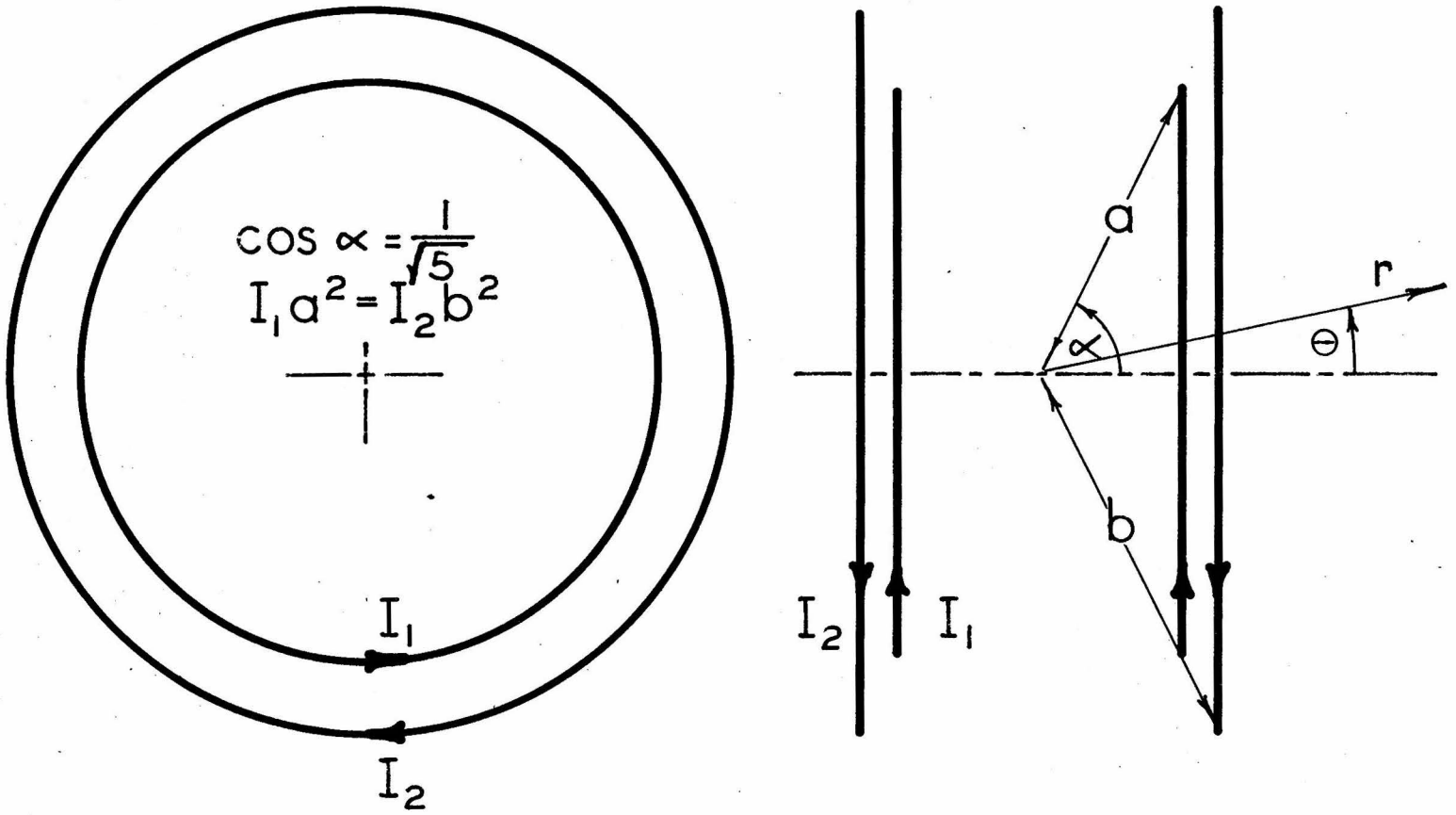

FIGURE 32. THE GEOMETRY AND NOMENCLATURE OF THE DOUBLE-HELMHOLZ SWEEP COILS.

The $n = 3$ term vanishes everywhere if one chooses $\alpha = \arccos 1/\sqrt{5}$, since $P_3^1(\cos\alpha)$ is zero for this value. This is the usual Helmholz condition.

The effect of the $n = 1$ term is made to vanish outside the coils by choosing $I_1a^2 = I_2b^2$. Hence, the dominant term in the expansion for the magnetic induction outside the coils then varies as the inverse seventh power of r.

The actual calculations are easiest with equations giving the fields in closed form (Ref. 24, p. 270, eq. 7.10 (6 and 7)). In general, complete elliptic integrals are involved, but the field along the axis is given by a simple algebraic expression.

REFERENCES

1. J. W. M. DuMond, Rev. Sci. Instr. 20, 160 (1949)

2. J. W. M. DuMond, L. Bogart, J. L. Kohl, D. E. Muller, and J. R. Wilts, Sp. Tech. Rep. No. 16 to the Res. Corp. and the O.N.R., C.I.T. (1952)

3. F. Bloch, Phys. Rev. 70, 460 (1946)

4. F. Bloch, W. W. Hansen, and M. Packard, Phys. Rev. 70, 474 (1946)

5. M. E. Packard, Rev. Sci. Instr. 19, 435 (1948)

6. N. Bloembergen, E. M. Purcell, and R. V. Pound, Phys. Rev. 73, 679 (1948)

7. A. Roberts, Rev. Sci. Instr. 18, 845 (1947)

8. N. J. Hopkins, Rev. Sci. Instr. 20, 401 (1949)

9. H. A. Thomas and R. D. Huntoon, Rev. Sci. Instr. 20, 516 (1949)

10. R. V. Pound and W. D. Knight, Rev. Sci. Instr. 21, 219 (1950)

11. H. A. Thomas, R. L. Driscoll, and J. A. Hipple, N.B.S.R.P. 2104 Vol. 44, June 1950; Phys. Rev. 78, 787 (1950)

12. F. E. Terman, Radio Engineers' Handbook, p. 505, Fig. 24(a), McGraw-Hill Book Company (1943)

13. R. H. Dishington, Proc. of the I. R. E. 37, 1401 (1949)

14. H. S. Sommers, P. R. Weiss, and W. Halpern, Rev. Sci. Instr. 20, 244 (1949)

15. Nuclear Data, Bureau of Standards Circular 499, September (1950)

16. G. Lindstrom, Phys. Rev. 83, 465 (1951)

17. H. Craig, Phys. Rev. 85, 688 (1952)

18. Y. Cauchois et H. Hulubei, Longueurs D'Onde des Emissions X et des Discontinuites D'Absorption X, Hermann and Cie, Paris, (1947)

19. R. D. Hill, E. L. Church and J. W. Mihelich, Tables of Critical X-Ray Absorption Energies, privately published. (1951)

20. J. W. M. DuMond and E. R. Cohen, Phys. Rev. 82, 555, (1951)

21. M. Siegbahn, Spektroskopie der Röntgenstrahlen, 2nd Ed., Julius Springer (1931)

22. D. J. Klein, Thesis, California Institute of Technology, (1951)

23. H. C. Hoyt, Thesis, California Institute of Technology, (1952)

24. W. R. Smythe, Static and Dynamic Electricity, 2nd Ed., p. 274, eq. 7.13(2), McGraw-Hill Book Company, (1950)